REPUPLIC OF TURKEY
ONDOKUZ MAYIS UNIVERSITY
GRADUATE SCHOOL OF SCIENCES

Design of Fractional Order Proportional-Integral-Derivative (FOPID) Controllers by Using 3-Dimensional (3-D) Plots

Mohamed Hassan Nor

MASTER'S THESIS

REPUPLIC OF TURKEY
ONDOKUZ MAYIS UNIVERSITY
GRADUATE SCHOOL OF SCIENCES

MASTER'S THESIS

Design of Fractional Order Proportional-Integral-Derivative (FOPID) Controllers by Using 3-Dimensional (3-D) Plots

Mohamed Hassan Nor

DEPARMENT OF ELECTRICAL AND ELECTRONICS ENGINEERING

SAMSUN
2019

Ethics declaration

I hereby declare that all the information on this thesis which are prepared in accordance with the thesis writing rules of Ondokuz Mayis University, graduate school of sciences. It contains accurate and complete information. I also have behaved in accordance with the scientific ethics in the course of the production of the information and cited all the sources that I have used.

14/06/2019

Mohamed Hassan Nor

ABSTRACT

Master's Thesis

Design of Fractional Order Proportional-Integral-Derivative (FOPID) Controllers by Using 3-Dimensional (3-D) Plots

Mohamed Hassan Nor

Ondokuz Mayis University

Graduate School of Sciences

Department of Electrical and Electronics Engineering

Supervisor: Assoc. Prof. Dr. Mehmet Emir KÖKSAL

Traditional proportional-integral-derivative (PID) and fractional order PID (FOPID) controllers are standard feedback control loop mechanisms that are commonly used today in many industrial applications. These controllers are designed to accurate the error between the reference and measured variables and to achieve the required output value, following the system design specifications. 3-dimentional plots and their use in designing ordinary PID or FOPID controllers have not been considered before in the literature on this extend.

In this thesis, a 3-D graphical method is developed to tune the gain parameters K_p, K_i, K_d of the FOPID controller knowing the fractional orders λ and μ. The method gives a graphical view of the acceptable control parameters satisfying the specified requirements on the 3- dimensional Euclid space $(K_p, K_i, K_d) \in R^3$. Although some design specifications in 2-dimentional plots have been given in the literature, this 3-D method has not been implied before. Also 3-dimensinoal plots, their mathematical and programming details as well as 3-D examples are not studied thoroughly in the literature.

For designing controllers by using this 3-D graphical method, system design specifications such as phase margin (PM), gain margin (GM), phase flatness (PF), output disturbance rejection (ODR) and high frequency noise rejection (HFNR) are considered and their important characteristics are shown.

Key words: PID controller, FOPID controller, Phase margin, Gain margin, Iso-damping, Noise rejection.

ÖZET

Yüksek Lisans Tezi

Kesirli Mertebeden Oransal-İntegral-Türev (FOPID) Denetleyicilerinin 3-Boyutlu (3D) Grafikler Kullanarak Tasarımı

Mohamed Hassan Nor

Ondokuz Mayis Üniversitesi

Fen Bilimleri Enstitüsü

Elektrik ve Elektronik Mühendisliği Anabilim Dalı

Danışman: Doç. Dr. Mehmet Emir KÖKSAL

Alışıla gelmiş oransal-entegral-türevsel (PID) ve kesirli mertebeden oransal-entegral-türevsel (FOPID) denetleyiciler günümüzde birçok endüstriyel uygulamalarda sıklıkla kullanılan standart geri beslemeli kontol döngüsü mekanizmalarıdır. Bu denetleyiciler, arzu edilen system tasarım özelliklerini sağlamak suretiyle referans değeri ve ölçülen işaret arasındaki hatayı ayarlamak ve istenilen çıkış değerini elde etmek için tasarımlanır. Üç boyutlu çizimler ve bunların alışıla gelmiş PID veya FOPID denetleyicilerin tasarımı için kullanılması, daha önce literatürde bu ölçüde ele alınmamıştır.

Bu tezde λ ve μ kesir mertebelerinin bilindiği farz edilerek, FOPID denetleyicilerin K_p, K_i, K_d kazanç parametrelerini ayarlamak için 3-boyutlu (3-D) grafiksel metod geliştirilmiştir. Metod, istenilen tasarım gereksinimlerini sağlayan kabul edilebilir kontrol parametrelerinin üç boyutlu $(K_p, K_i, K_d) \in R^3$ Euclid uzayında grafiksel görünümünü vermektedir. Literarürde 2-boyutlu uzayda bazı tasarım gereksinimleri verilmiş olmasına rağmen, bu tezdeki 3-D metodu daha önce ele alınmamıştır. Bu tezdeki 3-D çizimleri, bunların matemeatiksel ve programlama detayları ve örneklere uygulamaları daha önce literatürde detaylı olarak incelenmemiştir.

Önerilen 3-D metodu ile denetleyicilerin tasarımı için, faz aralığı (phase margin, PM), kazanç aralığı (gain margin, GM), faz düzgünlüğü (phase flatness, PF), çıkış bozucu bastırımı (output disturbance rejection, ODR) ve yüksek frekans gürültü bastırımı (high frequency noise rejection, HFNR) gibi tasarım gereksinimleri ele alınmış ve bunların önemli karakteristikleri gösterilmiştir.

Anahtar kelimeler: PID denteleyici, FOPID denetleyici, Faz aralığı, Kazanç aralığı, Bozucu bastırımı, Gürültü bastırımı.

ACKNOWLEDGEMENT

Firstly, I would like to give a special thanks to my supervisor Assoc. Prof. Dr. Mehmet Emir KÖKSAL for the special guidance, support, intellectual inspiration and for his personal maintenance throughout the period of this work. It was a boundless pleasure to me to work under his supervision. I am really and extremely grateful for his endurance and his continuous supervision during the whole period of this study of writing of this thesis.

I would also like to extend my sincere gratitude to all the academic staff in the department of Electrical and Electronics Engineering, specially the head of the department Prof. Dr. Okan ÖZGÖNENEL, Prof. Dr. İlyas EKER and Assist. Prof. Dr. Serap KARAGÖL for their kindly welcome and support.

Also I want to take this opportunity to show my gratefulness and love to my family who took the major part of this work and also for their endless encouragement and their financial support.

LIST OF FIGURES

LIST OF TABLES

TABLE OF CONTENTS

ABBREVIATIONS

FO	Fractional Order
PID	Proportional Integral Derivative
PI	Proportional Integral
PD	Proportional Derivative
FOPID	Fractional Order Proportional Integral Derivative
FDE	Fractional Derivative Equation
FIE	Fractional Integral Equation
FOS	Fractional Order System
LTI	Linear Time Invariant
GM	Gain Margin
PM	Phase Margin
CLS	Closed Loop System
RRB	Real Root Boundary
CRB	Complex Root Boundary
IRB	Infinite Root Boundary
DBU/L	Disturbance Boundary Upper/Lower
NBU/L	Noise Boundary Upper/Lower
FC/FS	Flatness Curve / Flatness surface
TP	Test Point
CPU	Central Processing Unit
GPMT	Gain Phase Margin Tester
GCOP/F	Gain Cross Over Point/Frequency
PCOP/F	Phase Cross Over Point/Frequency

1. INTRODUCTION

For the last decades, dynamical system controllers have been getting in numerous research interests which are constructed on fractional order (FO) calculus. It has been promoted that FO calculus will play a key role in a smart system. (Podlubny, 1998) proposed the concept of the FO Proportional Integral Derivate (PID) controllers and confirmed the efficiency of such controllers for activating the response of FO systems.

Fractional calculus is a term for the theory of integrals and derivatives of arbitrary orders, which combine and oversimplify the concepts of integer-order differentiation and n-fold integration (Podlubny, 1998).

1.1. Fractional Order System

A branch of mathematics that analysis the chance of changing the actual whole-number powers into a fractional (non-integer) order of derivatives and integrations is known as fractional calculus. There are different ways to describe fractional order operators of derivative and integrals. Fractional calculus has been studying since 1695. Because of its increasing facilitates of computational and the tools, fractional calculus has become a very important research topic. The equation that comprises fractional derivatives is called fractional differential equation (FDE), and the equation that contains fractional integrals is known as fractional integral equation (FIE) (Podlubny, 1998).

A system that contains FDE or FIE or both of these fractional equations is said to be a fractional order system (FOS). FOS is a very useful in a typical behavior of studying dynamic systems, in biology, chemistry and also chaotic system. In dynamic systems and the theory of control systems, fractional order is an essential tool that can be used for modelling FOS by using FDE and/or FIE that contains fractional orders.

Recently, applications with FOS have increased rapidly. The FOS, mathematically increases the accuracy of the real objects better than the traditional “integer order”

methods. The fractionality of many systems is very low even though the real objects are usually fractional (Nakagawa and Sorimachi, 1992). The absence of the fractional differential equations' solutions in explicit forms are the main reasons behind the usage of integer order methods.

Nowadays, Linear Time Invariant (LTI) systems with fractional orders, have attracted the intention of many control systems in the world, though, the investigations of the fractional order control systems have started in early 1960s (Manabe, 1960).

The general form of FOS can be written as

$$H(D^{\alpha_1,\alpha_2,\cdots,\alpha_m})(y_1, y_2, \cdots, y_m) = G\left(D^{\beta_1,\beta_2,\cdots,\beta_n}\right)(x_1, x_2, \cdots, x_n) \qquad (1.1)$$

where y_j and x_i are time domain output and input functions respectively, H and G are also functions of FD (fractional derivative) and D^{γ} is the fractional derivative operator, $\gamma = \alpha_1, \alpha_2, \cdots, \alpha_m$ and $\beta_1, \beta_2, \cdots, \beta_n$ are the orders of the fractional derivatives and generally these orders can be complex quantities.

A Linear Time Invariant system is a special case of Eq. (1.1) and this can be also modified as follows

$$\left(\sum_{i=0}^{m} a_i D^{\alpha_i}\right) y(t) = \left(\sum_{j=0}^{n} b_j D^{\beta_j}\right) x(t). \qquad (\mathbf{1.2})$$

Taking the Laplace transform of the LTI system of Eq. (1.2), the transfer function (TF) of the system is going to be as

$$TF = \frac{Y(s)}{X(s)} = \frac{\sum_{j=0}^{n} b_j S^{\beta_j}}{\sum_{i=0}^{m} a_i S^{\alpha_i}}. \qquad (\mathbf{1.3})$$

Generally based on the orders of $\propto_i$ and β_j of the transfer function, it can be said that FOS have unlimited memory potentially.

One of the motivations that encourages to study FOS is that dynamical systems are mostly described as exponential way and this exponential way are very classical approach and can be measure for the growth of population.

In (Rivero et al, 2011), it is stated that the order of a FOS is an admirable controller, and using this FO can be controlled how the target point is approached to or getting away from the target point.

1.2. PID Controller

Proportional integral derivative (PID) controller is a controller that has been used very widely and magnificently for the last several decades in various applications in industry and many other systems that need endlessly moderated controllers. What makes PID controller more widespread is its design simplicity and effectiveness (Podlubny, 1998).

A PID controller constantly computes the errors between the preferred set-point (SP) and the actual values of the system output which is called "process variable" (PV) and after calculating the error values the system will put on a correction based on the PID expressions. The proportional integral derivate (PID) controller produces an output that contains the combination of the results of proportional, integral and derivative controllers.

In real-world term, PID applies automatically and correct the responses to the controlled function. For daily practical example is going to be "cruise control" which is on the car, and this control system is effected externally. These external impacts decrease the speed of the car (such as peaks or hills). For the PID control system reinstates from present speed to the preferred speed in an optimum way, lacking of postponement or exceed, and this PID system restore is done just by controlling the car's engine output power. In the early 1920 s, automatic steering systems were the first theoretic study and applied application of PID controller and this steering system was developed for ships. Later it has been used widely for automatic procedure and for implementation in industrial manufacture, such as pneumatic, and electric controllers (Podlubny, 1998).

Nowadays, there are a lot of usage of the PID controller conception in the desires of demanding a precise and enhanced automatic control systems.

1.2.1. Block diagram of PID controller

The different appearance of PID controller is the capability to be able to use the combination of the controllers of proportional, integral and the derivative controllers to impacts on the control output to provide an occurrence and optimization of the desired output. Figure 1.1 shows the block diagram of the principles of the combined PID controller and how these three controller terms are combined.

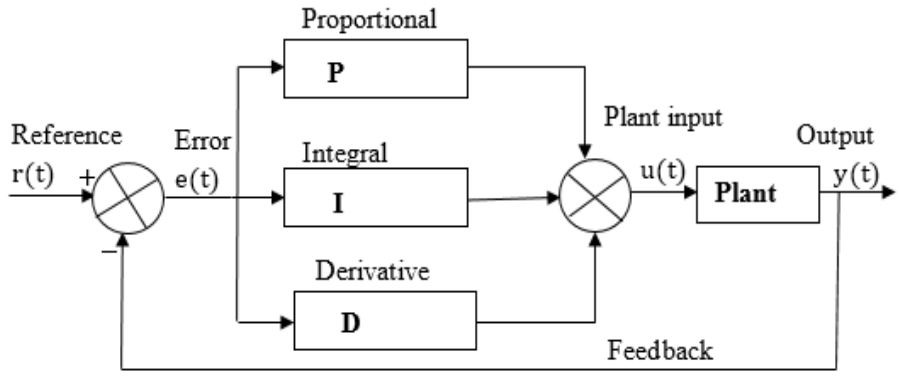

Figure 1. 1. Block diagram of a PID controller system

PID controller continuously computes the error $e(t)$, as mentioned before, considering the preferred set-point (SP) which is the reference point $r(t)$ and the measured values from the plant output $y(t)$, and according to the predefined reference value the system applies an improvement regarding the P, I and D control terms. Then the PID controller tries to lessen the error values by the modification of the controlled output as much as it can (Åström and Hägglund, 1995).

The error value that are proportional to the present value of the subtraction of plant output $y(t)$ from the reference value $r(t)$ is called proportional (P). P controller compares the preferred or the reference (set-point) with actual plant output value or the response procedure value. The consequential error value is multiplied by the proportional gain constant (K_p) to get the desired result. When the error value $e(t)$ is zero, then the output of this controller is also zero (Åström and Hägglund, 1995).

For instance, if there is a positive and a large value of error $e(t)$, then proportionally, regarding the gain factor K_p the control output will be large and positive. Using only P

controller with compensation, will consequence in $e(t)$ between the reference point $r(t)$ and the plant output value $y(t)$, because there is no error generated to have proportional answer there won't be any corrective reaction (Åström and Hägglund, 1995).

The integral controller accounts the error from the difference between the reference value and the plant output value of the previous error and integrates the difference over time to yield the integration (I). Due to the residual error values or the existence of the difference between the set-point value $r(t)$ and the actual plant output $y(t)$ variable which proportional (P) controller couldn't solve it, integral controller is required, to provide the essential accomplishment to diminish the residual error values or the steady state error.

Integral controller holds the final preferred value at which the difference between the reference value and the plant output reaches zero. When the error values go to negative value then the integral controller reduces its output. Integral controller limits the quickness of its response and this disturbs the stability of the system. The speed of integral controller response can be increased by reducing the K_i integral gain. For instance, if residual error is found after the proportional controller is applied, the integral controller (I) try to find out the solution of this residual error, by accumulating the effects of the integration for the cumulative error value. After the residual error is removed, the effects of integral controller will be stopped. This result will show the proportional consequence lessening as the error declines. When there is no need for high speed response, proportional-integral (PI) controller is used in most of the time (Podlubny, 1998).

P and I controllers don't have the ability to guess the upcoming performance of error. Derivative controller devastates this difficulty by predicting the upcoming performance of the system or error of the system. The best estimation of the future error result $e(t)$ from $r(t) - y(t)$, is done using the derivative (D) controller. The estimation is done based on the present error rate of alteration with respect to time and the constant K_d "derivative gain constant". Sometimes, derivative control is called "anticipatory control), because of its effect for trying to find out a reduction of the upcoming error $r(t) - y(t)$. So, by applying D controller effects the amount (rate) of error rate alteration (Åström and Hägglund, 1995).

So lastly PID is the combination of these three different controllers (proportional, integral and derivative), and this combination is done to have the best required response of the system.

1.2.2. Mathematical form of PID controller

Mathematically, the general PID controller output $u(t)$ is direct proportional to the proportional controller, the integral controller and the derivative controller, as can be seen from the equation below.

$$\mathrm{u(t)} \propto \left(\mathrm{e(t)} + \int_0^{\mathrm{t}} \mathrm{e(t)dt} + \frac{\mathrm{d}}{\mathrm{dt}}\mathrm{e(t)}\right). \quad \textbf{(1.4)}$$

Replacing the proportionality in Eq. (1.4) into proportional gain, integral gain and derivative gain constants, we have the general equation in time domain of the PID controller

$$\mathrm{u(t)} = \mathrm{K_P\, e(t)} + \mathrm{K_i} \int_0^{\mathrm{t}} \mathrm{e(t)dt} + \mathrm{K_d}\frac{\mathrm{d}}{\mathrm{dt}}\mathrm{e(t)} \quad \textbf{(1.5)}$$

where, K_p, K_i and K_d are constants, representing the proportional, integral and the derivative gain constants. Taking the Laplace transform on both sides of Eq. (1.5), we obtain

$$\mathrm{U(s)} = \mathrm{K_p E(s)} + \mathrm{K_i}\frac{1}{\mathrm{s}}\,\mathrm{E(s)} + \mathrm{K_d\, s\, E(s)}. \quad \textbf{(1.6)}$$

Factoring out $E(s)$ from the right side of Eq. (1.6) we can rewrite it as

$$\mathrm{U(s)} = \mathrm{E(s)}\left(\mathrm{K_p} + \mathrm{K_i}\frac{1}{\mathrm{s}} + \mathrm{K_d\, s}\right). \quad \textbf{(1.7)}$$

So, the transfer function of PID controller is going to be

$$\mathrm{G_c(s)} = \frac{\mathrm{U(s)}}{\mathrm{E(s)}} = \mathrm{K_p} + \mathrm{K_i}\frac{1}{\mathrm{s}} + \mathrm{K_d\, s} \quad \textbf{(1.8)}$$

$$= K_p\left(1 + \frac{1}{\tau_i s} + \tau_d\, s\right) \text{ where,} \quad \textbf{(1.9)}$$

$$\tau_{\mathrm{i}} = \frac{\mathrm{K_p}}{\mathrm{K_i}} \text{ and } \tau_d = \frac{\mathrm{K_d}}{\mathrm{K_p}}. \quad \textbf{(1.10)}$$

1.3. Fractional Order PID Controller

PID controllers have been used widely for the last decades in industrial applications, because of its simplicity structure and its well performance, and also because of its simple tuning in large range of conditional operations (Varol and Bingul, 2004).

Even though the control system theory has been developing, PID controllers are in use still for many industrial control systems (such as motor drivers, aerospace control, etc.). Dynamic systems such as FOS, and many other control systems have been considered as important research topics in various areas in engineering and science for the last decades.

FO controllers are defined by making the orders of the derivatives of the derivative controller and the integrals of the integral controller fractional (non-integer), and this can be easily control or modify the frequency response of the system straightly and unceasingly. Lacking of solution methods for the fractional differential equations were the main reasons behind the usage of integer-order models. But this disadvantage of FOC's has been overcome with the numerical techniques conducted by the developed high-speed digital computers.

Although, PID controller is one of the leading industrial controllers and hence PID controllers are matters of stable determination for the improvement of the system quality and the system robustness. One of the potentials to advance PID controllers is to habit the usage of fractional order controllers with non-integer derivatives and non-integer integration portions of the controller.

For the last few years industrial applications have been using systems that are containing derivatives with fractional order and integrals with fractional order (Vinagre et al, 2007). And different areas also have used fractional order controllers like electronics (Calderón et al, 2006), documentations of systems (Schlegel and Čech, 2004), robot manipulations (Ferreira and Machado, 2003), canal control for irrigations (Feliu-Batlle et al, 2007), Mechatronic-systems (Zhang et al, 2007; Ma and Hori, 2004) and heat control systems (Jesus and Machado, 2008).

It is important to mention that using FOS theory can compactly regulate and control many rising numbers of physical systems, and can be easily control these systems with

the help of FOPID controllers (Podlubny, 1999). Also FOPID controllers can be used even when the system has time delay behavior or is unstable (Hamamci and Koksal, 2010).

The generalization of traditional PID controller can be modified using fractional orders as $PI^{\lambda}D^{\mu}$, where λ and μ are the non-integers of the integrator-order and the derivative-order respectively.

Then the output response of the FOPID controller in time domain can be defined as:

$$u(t) = K_p\, e(t) + K_i\, D^{-\lambda}\, e(t) + K_d D^{\mu}\, e(t). \quad \textbf{(1.11)}$$

From Eq. (1.11), if $\lambda = 1$ and $\mu = 1$ then, we have normal conventional PID controller, if $\lambda = 1$ and $\mu = 0$ we have PI controller, and if and $\mu = 1$ and $\lambda = 0$ we have PD controller, and if both orders λ and μ are zero we only have proportional gain constants. These are different scenarios for the FOPID controllers design cases.

The continuous transfer function of the controller can be represented as

$$G_c(s) = \frac{U(s)}{E(s)} = \left(K_p + K_i \frac{1}{s^{\lambda}} + K_d\, s^{\mu}\right) = K_p\left(1 + \frac{1}{\tau_i s^{\lambda}} + \tau_d\, s^{\mu}\right), (\lambda, \mu \geq 0) \quad \textbf{(1.12)}$$

where τ_i and τ_d are given in Eq. (1.10).

Different from the standard PID, two extra parameters which are denoted λ and μ are additionally added. Scientists have indicated that these two additional parameters reinforce the system properties, and the pointer of the users, also these parameters increase the flexibility of the system and its stability.

When designing FOPID controllers, there are many factors that should be considered into account. Five different parameters $(K_p, K_i, K_d, \lambda, \mu)$ have to be considered for FOPID controller's specification design. Sometimes the required specifications for the controllers are generally to attain the load instabilities, frequency noises and the instability of the typical design mode.

So, under the consideration of all the tuning parameters $(K_p, K_i, K_d, \lambda, \mu)$ values of the FOPID controller, the optimum and the most appropriate solution of the system can be reached.

FOPID controller is a useful configuration that has been active for control dedications. FOPID controller is constructed by using the abovementioned five parameters which are the proportional, integral and the derivative gain constants *(K_p , K_i, K_d)* and the fractional integral and the derivative orders (λ, μ) of the system respectively.

At the first time, fractional-order proportional integral derivative controller is studied by (Podlubny, 1999), since then the researches about the FOPID controllers have been increasing continuously (Boudjehem and Boudjehem, 2013; Kheirizad et al, 2013; Kheirizad et al, 2012; Ghasemi et al, 2014; Cao, 2006; Özbay et al, 2012; Dimeas et al, 2017; Li et al, 2010; Li and Chen, 2008; Luo et al, 2010; Padula and Visioli, 2011; Shah and Agashe, 2013).

1.3.1. Genetic algorithms for PID and FOPID controllers

There are different studies for FOPID and PID controllers' design algorithms in the past researches. Bingul and Karahan has developed a method to get the optimal values of the parameters of the FOPID controller for robot trajectory control, considering given restrictions (Bingul and Karahan, 2012). This method is an easy method and since the reliability is high it has future potential for the control zone.

It is not easy to optimize the FOPID controller's parameters $(K_p, K_i, K_d, \lambda, \mu)$ of linear systems and non-linear systems. It is essential to have a global approach automatic optimization parameters in order to have efficient and effective FOPID controllers.

Numerous evolutions for parameter's optimization algorithms have been developed for the last decades, such as genetic algorithms (Chang and Chen, 2009; Aldair and Wang, 2010; Lee and Chang, 2010). Bingul (2004), has proposed a differential evolution algorithm (DEA) for PID controller design, to have a stable reference point and to provide an integrating procedure with time domain and this is one of the important algorithms for PID controllers. The evolution of the differential algorithm has recently upgraded and realized that this is a very dominant algorithm for the optimization of the FOPID controller's parameters. In (Biswas et al, 2009), Biswas et al. have suggested that differential evolution algorithms have very useful effects on the FOPID controller containing fractional derivatives and the fractional integrals. The parameters of FOPID

controller containing the three constants of proportional, integral and the derivatives gain constants and the orders of the integrals and the derivatives have been designed in a different way than the traditional PID controller making the integer order fractional orders that make the system more complex.

Smart optimization for designing FOPID controllers based on the particle swarm optimization (PSO) is proposed in (Cao and Cao, 2006; Maiti et al, 2008). Based on this approach, FOPID controller can be designed with the help of fractional calculus and this can give the FOPID controller high-performance.

To design the FOPID controller parameters, PSO is used and this promises the position of the particles. Zamani et al. have proposed and studied a FOPID controller to control automatic voltage regulator (AVR) (Zamani et al, 2009). In this study PSO algorithm is used to transfer the above-mentioned design process. The PSO algorithms is a progressive research process that has been demonstrated to have actual high effectiveness. Both time domain and the frequency domain control strategy is facilitated by using this PSO algorithms.

Nevertheless, FOPID controller's design complication increased, because of the fractional orders of derivative and integrals in contrast with the conventional PID controller.

Adaptive PSO (APSO) algorithm which is a method intended to control the system parameters and the system parameter's optimization is proposed in (Alfi and Modares, 2011). In the proposed method, each particle is adjusted dynamically with inertia weight considering the previous best memories of each feedback. The main compensations of the suggested "APSO" algorithm are to accomplish more rapidly convergence-speed and enhanced resolution precision with smallest incremental computational responsibility.

Closed loop system with time delay plant of PI controller have been proposed by (Yüce et al, 2016) using a relay automatic tuning tests, the final frequency of the system is achieved, after that using the received frequency the parameters of the PI control system are estimated from the tuning formula of Ziegler-Nichols (Z-N). The process of finding the parameters of the system is known as tuning. The Ziegler-Nichols (Z-N) method of finding the parameters of both open loop and closed loop control systems of PI and PID

controllers are still in use and it is a widespread turning formula. The consequence of changing the fractional integrator order (λ) by using the profound parameter's values for FOPI controller of a closed-loop system, the system step response is observed and according to the varying λ values, the proposed study has shown that using fractional order PI controller is more desired then the normal PI controller.

In (El-Khazali, 2013), El-Khazali proposed a new method to design FOPD controller and the FOPID controller. Using biquadratic approximation of FO differential operator, a fresh construction of predictable order of FOPID are suggested. This FOPID control has less tuning parameters then the conventional tuning parameters. Also using this fractional order PD controller, the system can attain the preferred phase-margins lacking of transferring the gain crossover-frequency of the un-controlled system.

Both traditional PID controller and the FOPID controllers have gained a significant care for the last few years both in industrial and educational researches (see the references (de Oliveira Valério, 2005; Micharet, 2006; Vinagre et al, 2007; Monje et al, 2008) for more details). According to these researches, FOPID controller provides the traditional PID control systems more flexibility, more reliability, because of the five parameters that FOPID controllers have, instead of having only three parameters as the conventional PID controllers. However, this increase of parameters also increases the complexity of the system tunings parameters. So, in order to solve these FOPID controller's tuning parameters problem, various methods have been used for designing FOPID controllers in the last years as aforementioned in (Maiti et al, 2008a; Biswas et al, 2009; Zamani et al, 2009).

It is conversely accepted that, for the FOPID extensive use in engineering, FOPID controllers should maintain the similar easiness of the traditional PID controller and it should clearly provide the enhancement of FOPID controller's performance and show that they are better than the traditional PID controllers. Increasing the tuning rules is one of these advantageous success of the traditional PID controllers (O'Dwyer, 2009). Also according to (Åström and Hägglund, 2006) to make the tuning parameters automatic is another important reason for the FOPID controller design success. Considering these

reasons, the tuning rules for fractional order PID controller is essential issue (Sánchez et al, 2017)

Choosing an appropriate tuning parameters is very important for designing an effective control system algorithm, depending on this parameter selection, model structure can be modified according to the desired systems. It is out of question that selecting the best parameters and making the best approximation lead the system to have better yields for forming progression. (Senberber and Bagis, 2018) Proposed two different modeling parts. The first one is to design an integer-order system model using "differential evolution algorithm (DEA) and "artificial bee colony" (ABC), and this is done using integer and fractional model constructions with time delays. The second part is done using a new prototype attained with the assistance of matlab/simuling set, to design a FOPID controller. ISE (integrated square error) modeling procedure is chosen as the presentation error criteria.

According to the result of this research, fractional-order exhibition has attained the enhanced result than the integer-order modeling. Also, the first part of the two modeling study parts or the design algorithms have better suitable performance. Furthermore, Senberber and Bagis have proposed a detailed debate on the FOPID controller's system performance using ABC algorithms for a non-integer order systems (Senberber and Bagis, 2017).

On the other hand, Bağiş and Senberger have presented a study that tests the system performance of high order modeling system using ABC algorithms (Bağış and Senberber 2016). Another system model is presented in (Mete et al, 2016) establishing on cascade of a linear model and non-linear second order volterra (SOV) model using differential evolution algorithms.

In (Azar and Serrano, 2018), Azar and Serrano have proposed a slide mode of FOPID controller and an observer that intends for the non-linear continuous stabilization. The system design and the observer scheme is done in an isolated style. PSO algorithm is used for the tuning parameter designs, especially to develop and select the integral order (λ) and the derivative order (μ) parameters. Lastly, in synchronous switching closed-loop system stability is guaranteed.

Integer-order PID controller and the FOPID controller are proposed in (Chopade et al, 2018). This study is for to control the levitated objects in their position in (magnetic levitation system), and this system is naturally a non-linear and unstable system.

The traditional integer-order such as PD controller and the PID controllers have been implemented in industrial applications more than 50-years, and these controllers are used for controlling linear and non-linear systems (Åström and Hägglund, 1995). For the last years, conventional PID controller and the FOPID controllers have been prolonged to their general forms with the help of fractional differentiation and fractional integration of arbitrary orders (Podlubny, 1999; Das, 2008). (The transfer function of the fractional-order is approximated by integer-order transfer function using different methods (Podlubny, 1999; Charef et al, 1992; Oustaloup et al, 2000)).

The strange action of the brain cells sources an epilepsy which is a dynamic disorder of the brain at the system level. A closed loop control system is proposed by Soltan et al. to identify the epileptic appropriations and to destroy it through stimulating the brain cells (Soltan et al, 2018). According to that study, PID is the most widely used "closed-loop" controller, due to the simplicity of the implementation and the system robustness of PID controller. The study use FOPID controller. Using the FOPID controller, various stability of the system domains were established based on the non-integer order and therefore, because of the increased parameters the freedom of the system also increased. ("Neural mass model (NMM)" is used to exam the stage for the controller for suppressing the brain activity). Luo et al. have defined that "Brain neurological disorders such as epilepsy are dynamical disorders due to abnormal activities of the brain cell" (Luo et al, 2017). It is difficult to cure abnormal activity and such an illness of brain cells using open loop frontward stimulation techniques because of its dynamic behavior and unpredictable. So closed-loop controllers were preferred to identify the abnormality and then via the control algorithms the controller selects to beat these abnormality (Salam et al, 2016; Wang et al, 2016). Furthermore, an important amount of studies have been completed using fractional-calculus in various research zones (Ali et al, 2013; Freeborn et al, 2013; Saha et al, 2013).

Actually, the FOPID controller has been recognized earlier in the application control theory and this demonstrates a huge flexibility in the system tuning-parameters and the system design (Caponetto, 2010).

On behalf of the flexibility of FOPID controllers, there are some difficulties for designing fractional controllers in time-domain. Furthermore, it has been detected that the procedures centered at the "gain" and the "phase" margins presenting in the past studies for conventional order systems are not totally appropriate to the FOS. According to identified gain and the phase margins, stability regions of FOPID controllers were studied by Cokmez et al. in order to control the integrating procedure with time domain obtaining and visualizing in the plane (Cokmez et al, 2018). In that study, the fractional integral of arbitrary order (λ) were assumed to be varying from 0.1 to 1.7. According to the values of the arbitrary order of the integral order (λ), and the different phase and gain margins, various stability areas have been gained.

Because of the two extra additional parameters (λ, μ), FOPID controllers have more effective performance than the traditional integer-order PID controllers (Zheng et al, 2017) .

In (Ren et al, 2018), Ren et al. have proposed a FO system model of "pneumatic servo system" by changing the dynamic equations of the integer-orders into a fractional-order equations. Then the FOPID controller is improved for the "servo system" by using "an online multi-variable multi-objective genetic algorithm (MMGA)". And in order to have comparable results the study also have used the traditional integer-order PID controller with the same method.

FOPID controllers with variable-orders have been studied in (Dabiri et al, 2018) using for linear dynamic systems. In this study a method to discretize the FDE with the variable-operators have been suggested. To find the optimum tuning parameters PSO algorithm is used in this research article. Three different examples have been done in the research and these three results have shown that fractional order-PID controller have more effective than the conventional PID controllers.

1.3.2. Optimization methods for PID and FOPID controllers

For the closed loop control systems viewpoint, asymptotic following of various forms of set-point inputs (for example step and ramp) are some of the noticeable objectives of control systems (Tavazoei, 2010). To control the system performance, integral performance indices are considered, and the integral indices are established on the system error, also time is regarded as a computable measure of the closed (feedback) loop systems.

A system controller is on its optimal, when the system parameters are tuned to values such that the pre-required design restriction are met, and when the integral indices touches its lowest point. In time domain performance criteria, some of the familiar integral indices of PID and FOPID and some other control structures include “Integral Absolute Error (IAE)”, “Integral Time Square Error (ITSE)”, “Integral Time Absolute Error (ITAE)”, “Integral Square Error (ISE)”, “Integral Square Time Error (ISTE)” and “Integral Square Time Square Error (ISTES)”. The mathematical formulation of these integral performance indices are given as (Das et al, 2011).

$$\mathrm{IAE} = \int_0^\infty |e(t)|dt \tag{1.13}$$

$$\mathrm{ITSE} = \int_0^\infty te^2(t)dt \tag{1.14}$$

$$\mathrm{ITAE} = \int_0^\infty t|e(t)|dt \tag{1.15}$$

$$\mathrm{ISE} = \int_0^\infty e^2(t)dt \tag{1.16}$$

$$\mathrm{ISTSE} = \int_0^\infty t^2e^2(t)dt \tag{1.17}$$

$$\mathrm{ISTES} = \int_0^\infty [t^2e(t)]^2dt. \tag{1.18}$$

The fact is that each of the different types of integral performance indices, has its particular advantages in control system design (Rajasekhar et al, 2014). According to (Rajasekhar et al, 2014), ITSE has the most benefits of punishing the system error further, and also because the presence of time multiplication term, ITSE restrains out the system oscillation very rapidly. Conversely, when unexpected alterations occur in the reference point, ITAE based controllers are preferred.

Nevertheless, the time-multiplication term in ITAE integral indices disciplines the error further at future or later steps, and supports reducing the settling-time T_s which is defined as the time that elapses for the output to remain near the reference value with an error less than $\mp 5\%$. Also the absolute error that take in the ITAE is for minimizing the overpass.

For PID and FOPID optimal design, different smart techniques have been suggested by (Das et al, 2013) in order to diminish the integral performance indices. ITAE is used for FOPI control system design in a permanent magnet synchronous motor using HDABCA "Hybrid Differential Artificial Bee Colony Algorithm" by (Rajasekhar et al, 2014).

Optimizing the ITAE with the PSO algorithm have been established by (Maiti et al, 2008b) for PID and FOPID control system design stability. (Cai et al, 2009) proposed a very useful application of ITAE using different evolutionary algorithms based on the FO system controllers. The advantage of ISE and ITAE have been confirmed by (Xue et al, 2006) in the existence of non-linearity, using a test-bed as a DC-motor. The study was examined for a "position-servo-mechanism" control systems regarding the actuator-saturation and the system-flexibility of shaft-torsional.

Freshly few scientists, separately from regarding the aforementioned error placed metrics, likewise concentrated on lessening the control signal. For example, Integral Square Controller Output (ISCO) and also Integral Square Deviation Controller Output (ISDCO) are the best and most extensively used ones.

(Cao et al, 2005) have used genetic algorithm to improve and find the best controller's parameters and to optimize weighted sum of ISE and ISCO. Furthermore, Cao et al. have used PSO for the similar application.

Revolutionary, researches involved combining of the "time integrals and the controller's integrals and their tunings by several evolutionary-algorithms for application alternating from the plant control, multiple-input multiple-output (MIMO) systems, network control systems chaotic systems can be found in" (Pan and Das, 2013). Different from the evolutionary and PSO based design, another important way of designing FOPID controller is for Fuzzy instructions (Das et al, 2012).

In the time domain optimization methods of controller design, the error function $e(t) = r(t) - y(t)$ is not the only objective to minimize. There are other performance indices. Different from the time-integrals, (Biswas et al, 2009) proposed an optimization method using "Differential Evolutions", for the problem optimizations of FOPID controllers such as "dominant pole-placement". PSO based optimizations outline has been designed by (Kadiyala et al, 2009) in order to minimize the "weighted sum, rise-time, overshoot, settling-time steady-state-errors" of the FOPID control systems. Some other approaches for minimization and system optimization can be found in (Zamani et al, 2009; Rajasekhar et al, 2012; Pan and Das, 2012; Das et al, 2011).

The advantage of the ITAE has the ability to produce small overshoot and oscillations compared to the IAE and the ISE performances. And according to the ITAE has the best selectivity and sensitivity compared to the IAE and ISE (Schultz and Rideout, 1961) "In contrast to ITAE, ITSE has also les sensitivity and it is not contented computationally" (Maiti et al, 2008b) .

2. FRACTIONAL ORDER CALCULUS

The branch of mathematics, that is the study of the chances of describing the real or the complex number of powers of a differential operator and the integral operator (D and I) is called Fractional calculus. The generalizations of basic differentiation and integration into a non-integer order operator (${}_{a}D^{\alpha}_{t}$) equations are referred as a fractional calculus or sometimes it is called "extraordinary differential equations". Where a and t are the boundaries of lower and upper limits of the integration respectively also, D is the operator and α is the operator order ($\alpha \in R$).

The representation of differential operator and the integral operator are shown in Eq. (2.1) below, and this evolves the generalization of an integer calculus operators.

$$\mathrm{D}\ \mathrm{f(t)} = \frac{\mathrm{d}}{\mathrm{dt}}\mathrm{f(t)},\ \ \mathrm{I}\ \mathrm{f(t)} = \int_0^{\mathrm{t}} \mathrm{f(t)dt}. \qquad \textbf{(2.1)}$$

More usually, this fractional calculus can be defined as the linear function D^{α}, and if the power of the operator (D) is a real number, such that if the operator has an integer value $\alpha > 0$ and $\alpha = n \in Z$ it agrees coincidently with the normal differentiation and if $\alpha < 0$ and $\alpha = n \in Z$ this means that negative power of operator (D) agrees with the normal integration (I).

2.1. Fractional Derivative of the general power

Consider and assume the monomial $f\ (x)$ has the form of

$$\mathrm{f(t)} = \mathrm{x}^{a}. \qquad \textbf{(2.2)}$$

If we take the first derivative and write the usual form of the first derivative, the above function is going to be as

$$\mathrm{f}'(\mathrm{x}) = \frac{\mathrm{d}}{\mathrm{dx}}\mathrm{f(x)} = \mathrm{ax}^{\mathrm{a}-1}. \qquad \textbf{(2.3)}$$

And taking the derivative of Eq. (2.3) once again, it will give more general formula of that

$$\frac{d^n}{dx^n}x^a = \frac{a!}{(a-n)!}x^{a-n}. \quad \textbf{(2.3)}$$

Before replacing the factorial with the gamma function, let's first see and define the gamma function.

In mathematics, one of the most important function of factorial calculus is called gamma function or Euler's gamma function. The Greek letter of Γ is denoted by the gamma. Certainly, this Euler's gamma function $\Gamma(z)$, is an extension of a shifted 1 to real or complex numbers down for the factorial function which generally allows the factorial n! to have a non-integer or a complex value.

The definition of Euler's gamma function $\Gamma(z)$, is defined as follows:

$$\Gamma(z) = \int_0^\infty e^{-t}t^{z-1}dt. \quad \textbf{(2.4)}$$

This integral converges when the real part of z (complex number) is positive $Re\ (z) > 0$. Assuming that $z = x + iy$, and substituting in Eq. (2.4) we are going to have

$$\Gamma(x+iy) = \int_0^\infty e^{-t}\,t^{x-1+iy}dt = \int_0^\infty e^{-t}\,t^{x-1}\,e^{iylog(t)}dt$$

$$= \int_0^\infty e^{-t}\,t^{x-1}\,[\cos(ylog(t)) + i\sin(ylog(t))]dt. \quad \textbf{(2.5)}$$

Having look at Eq. (2.5), when $t = 0$ we have only the real number $Re(z)$ which is equal to 1 and when $t = \infty$ we have e^{-t} in the square brackets.

The gamma function satisfies the following equation

$$\Gamma(z+1) = z\Gamma(z). \quad \textbf{(2.6)}$$

Using the gamma function formula which is given in Eq. (2.4) and using the integration by part then, Eq. (2.6) can be proved.

Clearly, $\Gamma(1)$ is going to be 1 and by using Eq. (2.6), we can conclude that when $z = 1, 2, 3, 4, \cdots$,

$$\Gamma(2) = 1.\Gamma(1) = 1.0! = 1!$$
$$\Gamma(3) = 2.\Gamma(2) = 2.1! = 2!$$
$$\Gamma(4) = 3.\Gamma(3) = 3.2! = 3!$$
$$\cdots \quad \cdots \quad \cdots$$

$$\Gamma(n+1) = n.\Gamma(n) = n.\Gamma(n-1)! = n!$$

Finally, we can write this as $\Gamma(n) = 1.2.3.4 \cdots (n-1) = (n-1)!$ for all positive integers. Now going back to Eq. (2.3) and substituting the factorial part with the gamma function (Euler's gamma function), we have

$$\frac{\mathrm{d}^{\mathrm{n}}}{\mathrm{dx}^{\mathrm{n}}}\mathrm{x}^{\mathrm{a}} = \frac{\Gamma(\mathrm{a}+1)}{\Gamma(\mathrm{a}\ -\ \mathrm{n}+1)}\ \mathrm{x}^{\mathrm{a}-\mathrm{n}}, \qquad (\mathrm{a} \geq 0). \tag{2.7}$$

For example, assuming that $a = 1$ and $n = 1/2$, and substituting into Eq. (2.7), we obtain

$$\frac{\mathrm{d}^{1/2}}{\mathrm{dx}^{1/2}}\mathrm{x} = \frac{\Gamma(1+1)}{\Gamma(1-1/2+1)}\mathrm{x}^{1-1/2} = \frac{\Gamma(2)}{\Gamma\left(\frac{3}{2}\right)}\mathrm{x}^{1/2} = \frac{2\mathrm{x}^{1/2}}{\sqrt{\pi}}.$$

Taking half derivative again, we have to get the first derivative of function $f(x)$ as expected;

$$\frac{d^{1/2}}{dx^{1/2}}\frac{2x^{1/2}}{\sqrt{\pi}} = \frac{\Gamma(1/2+1)}{\sqrt{\pi}\,\Gamma(1/2-1/2+1)}x^{1/2-1/2} = \frac{\Gamma(3/2)}{\sqrt{\pi}\,\Gamma(1)}x^{0} = 1.$$

Knowing that $\Gamma(1) = 1$ and $\Gamma(3/2) = \frac{\sqrt{\pi}}{2}$ this is the similar of taking the first derivative of the function $f(x) = x$ then

$$\left(\frac{d^{1/2}}{dx^{1/2}}\frac{d^{1/2}}{dx^{1/2}}\right)x = \frac{d}{dx}x = 1.$$

On the other hand, if the integer power of a is a negative number, then gamma function is undefined so, the following relationship is valid in that case.

$$\frac{\mathrm{d}^{\mathrm{n}}}{\mathrm{dx}^{\mathrm{n}}}\ \mathrm{x}^{-\mathrm{a}} = (-1)^{\mathrm{n}}\frac{\Gamma(\mathrm{a}+\mathrm{n})}{\Gamma(\mathrm{a})}\mathrm{x}^{-(\mathrm{a}+\mathrm{n})}, \text{for a} \geq 0. \tag{2.8}$$

Because of the undefined gamma function when the real part of a is a negative integer and the imaginary part is zero, "it is required to do the fractional derivative after the integer derivative has been performed". For instance, if you have such a fractional derivative $D^{\frac{3}{2}}f(x)$ the following way should be performed.

$$\mathrm{D}^{\frac{3}{2}}\mathrm{f(x)} = \mathrm{D}^{1/2}\ \mathrm{D}^{1}\ \mathrm{f(x)} = \mathrm{D}^{1/2}\frac{\mathrm{d}}{\mathrm{dx}}\ \mathrm{f(x)}.$$

2.2. Mathematical Formulation of Fractional Order Calculus

Among different definitions of fractional order fundamental operators, three commonly used definition formulas, are considered in this section.

2.2.1. Grunwald-Letnikov (GL) fractional definition

Grunwald-Letnikov (GL) fractional definition is one of the most important and fundamental definitions for the fractional calculus. Taking $[a\ t]$ as the lower and the upper limits, the GL fractional definition is define as

$$aD^{-\alpha}{}_t f(t) = \lim_{h\to 0} h^{-\alpha} \sum_{i=0}^{\left[\frac{t-\alpha}{h}\right]} (-1)^i \binom{\alpha}{i} f(t-ih), \qquad (\mathbf{2.9})$$

where $[\cdot]$ is the integer-part and $\binom{\alpha}{i} = \frac{\alpha(\alpha-1)(\alpha-2)\cdots(\alpha-i+1)}{i!}$ is the binomial coefficients notation.

2.2.2. Riemann-Liouville fractional definition

One of the fractional calculus classic forms is given by Riemann-Liouville (RL). The RL fractional definition is a very fundamental and important equation for the fractional calculus. Especially, for the boundary conditions and the repetition functions which is called periodic function is considered in RL equation. Similar to the GL there exist lower and upper limits for the RL fractional calculus definition $[a\ t]$. The general form of RL fractional differ-integral is given as:

$$aD^{\alpha}{}_t f(t) = \frac{1}{\Gamma(n-\alpha)} \left(\frac{d}{dt}\right)^n \int_a^t \frac{f(\tau)}{(t-\tau)^{1-(n-\alpha)}} d\tau. \qquad (\mathbf{2.10})$$

It is essential to mention that n is the smallest integer that is greater than or equal to α such that $n-1 < \alpha < n$, and $\Gamma(\cdot)$ is the familiar Euler's gamma function.

2.2.3. Caputo's fractional definition

In 1967 M. Caputo introduced in a paper a different method of calculating fractional derivatives. Comparing Riemann-Liouville's fractional derivative definition, when it comes to solve differential equations Caputo's fractional derivatives do not need the initial condition's definition of the fractional order. Caputo's fractional derivative definition is very popular and most of the systems use Caputo's definition given below.

$$ {}_{0}D_{t}^{\alpha} = \frac{1}{\Gamma(\alpha - n)} \int_{a}^{t} \frac{f^{(n)}(\tau)d\tau}{(t-\tau)^{\alpha+1-n}} \quad \text{for } n-1 < \alpha < n. \tag{2.11} $$

If $\alpha = n$ then the Caputo's definition turns to a classical form as

$$ {}_{0}D_{t}^{\alpha} = \frac{d^{n}}{dt^{n}} f(t) \quad \text{for } \alpha = n. \tag{2.12} $$

where n is the smallest integer that is greater than or equal to α.

2.3. Laplace Transform of Fractional Calculus

In most system concepts, the study of dynamical manners is frequently prepared by means of transfer-functions. The overview of the Laplace transform of the fractional order derivatives is essential for an optimum training. Luckily, not a huge variance can be established with admiration to the conventional occasion, approving the usefulness of the Laplace transform mathematical implement even for the non-integer order systems. The very basic definition of Laplace transform is

$$ F(s) = \mathcal{L}\{f(t)\} = \int_{0}^{\infty} e^{-st} f(t)dt \tag{2.13} $$

where s is a complex number.

Coming back to the Laplace transform of the fractional order, the most overall formulation is given as

$$ \mathcal{L}\{D^{\alpha} f(t)\} = s^{\alpha}\mathcal{L}\{f(t)\} - \sum_{k=0}^{n-1} s^{k} \left[\frac{d^{\alpha-1-k} f(t)}{dt^{\alpha-1-k}}\right]_{t=0} \tag{2.14} $$

where n is an integer number, such that $n-1<\alpha<n$. We can also state that Eq. (2.14) is the general form of the fractional order derivatives. This equation converts to a very easy way, when the initial (derivative part) condition is zero.

$$\mathcal{L}\{\mathrm{D}^{\alpha}\mathrm{f}(\mathrm{t})\}=\mathrm{s}^{\alpha}\mathcal{L}\{\mathrm{f}(\mathrm{t})\}. \tag{2.15}$$

On the other hand, the Laplace transform of the integration can be expressed as below, starting from the first integration.

$$\mathcal{L}\{\mathrm{Df}(\mathrm{t})\}=\mathcal{L}\left(\int_0^{\mathrm{t}}\mathrm{f}(\tau)\mathrm{d}\tau\right)=\frac{1}{\mathrm{s}}(\mathcal{L}\{\mathrm{f}\}).$$

For the second and third operators of the Laplace transform are

$$\mathcal{L}\{\mathrm{D}^2\,\mathrm{f}(\mathrm{t})\}=\frac{1}{\mathrm{s}}(\mathcal{L}\{\mathrm{Df}(\mathrm{t})\})=\frac{1}{\mathrm{s}^2}(\mathcal{L}\{\mathrm{f}\})$$

$$\mathcal{L}\{\mathrm{D}^3\,\mathrm{f}(\mathrm{t})\}=\tfrac{1}{\mathrm{s}^2}(\mathcal{L}\{\mathrm{D}^2\mathrm{f}(\mathrm{t})\})=\tfrac{1}{\mathrm{s}^3}(\mathcal{L}\{\mathrm{f}(\mathrm{t})\})\text{ and so on.}$$

And this provides the general formula of the fractional integral calculus formula as

$$\mathcal{L}\{\mathrm{D}^{\alpha}\,\mathrm{f}(\mathrm{t})\}=\tfrac{1}{\mathrm{s}^{\alpha}}(\mathcal{L}\{\mathrm{f}\}). \tag{2.16}$$

Note that α can be a non-integer number.

Undoubtedly, Laplace transform is a very useful tool for solving fractional DE. For instance, the convolution rule in time domain becomes a multiplication in frequency domain, and this is done with the help of Laplace Transformation.

$$\mathcal{L}\{\mathrm{f}(\mathrm{t})*\mathrm{g}(\mathrm{t})\}=\mathcal{L}\{\mathrm{f}(\mathrm{t})\mathrm{g}(\mathrm{t})\}. \tag{2.17}$$

For example, assuming that there are two functions of $f(t)$ and $g(t)$, where $g(t)=x^{\alpha-1}$, using Cauchy Laplace transform, we obtain

$$\left(\mathrm{D}^{\alpha}\,\mathrm{f}(\mathrm{t})\right)=\frac{1}{\Gamma(\alpha)}\mathcal{L}^{-1}\left\{\mathcal{L}\{\mathrm{g}(\mathrm{t})\}\,\mathcal{L}\{\mathrm{f}(\mathrm{t})\}\right\}=\frac{1}{\Gamma(\alpha)}\left(\mathrm{g}(\mathrm{t})*\,\mathrm{f}\,(\mathrm{t})\right)=\frac{1}{\Gamma(\alpha)}\int_0^{\mathrm{t}}\mathrm{g}(\mathrm{t}-\tau)\;\mathrm{f}(\tau)\mathrm{d}\tau$$

$$=\frac{1}{\Gamma(\alpha)}\int_0^{\mathrm{t}}(\mathrm{t}-\tau)^{\alpha-1}\mathrm{f}(\tau)\mathrm{d}\tau.$$

2.5. Fractional Order System Stability

For the last decades, fractional calculus application theories have become a desirable development. Various researchers have been studying on the dynamic system control stability and the FOS stability. However, because of the huge determinations in a short time, offerings are distributed beside the past study, and to have a whole picture of today's FOS become hard for the researchers.

Stability is a very essential factor for dynamic systems that can be considered both in time domain and in frequency domain.

2.5.1. Time domain stability criterion

The general notion of bounded-input bounded-output (BIBO) system stability can be considered in time domain and can be stated or defined through the bellow conditions (Petras, 2008). A causal LTI system which has the impulse response of $h(t)$ must satisfy the condition below in order to be BIBO system stable.

$$\int_0^\infty ||h(\tau)||d\tau. \qquad \textbf{(2.18)}$$

The output $y(t)$ of the systems in time domain is the convolution of the LTI system input $x(t)$ and the system impulse response $h(t)$. An LTI system is a causal system, only if the system output depends on the past and the present input values and not its future values (Matignon, 1998).

$$y\,(t) = x(t) * h(t) = \int_0^\infty h(\tau)\, x\,(t-\tau)d\tau. \qquad \textbf{(2.19)}$$

2.5.2. Frequency domain stability criterion

Frequency domain representation is very important demonstration of stability. Let a SISO system be represented by the transfer function between its input and output as in Eq. (1.3). For the stability of the system it is required that all the poles of this transfer function, that is the roots of the characteristic equation

$$\sum_{i=0}^{m} a_i s^{\alpha_i} = 0 \qquad (\mathbf{2.20})$$

should be in the left half of the complex s-plane. To check this, algebraic methods such as Routh Hurwitz standards can't be used directly in FOS because, in FOS we have multivalued function also known as "pseudo polynomial with rational power" instead of having polynomial characteristic that can be used for Routh Hurwitz. In some special situations it might be possible (Ahmed et al, 2006). Furthermore, linear matrix inequality method and some other algorithms have been used for modern control systems (Oustaloup et al, 2008; Hamamci, 2008; Hwang and Cheng, 2006).

Nevertheless, an exact s- domain stability test like Routh Hurwitz Criterion can be used to test the stability of commensurate FOSs. For illustrating commensurate case consider the Caputo fractional derivative D^{α}, let us have a look at the fractional order LTI system. The state space model of the fractional order LTI system can be written as follows.

$$\mathrm{D}^{\alpha}\mathrm{x} = \mathrm{Ax} + \mathrm{Bu} \qquad \textbf{(2.21)}$$

$$\mathrm{y} = \mathrm{Cx} \qquad \textbf{(2.22)}$$

where $x, u,$ and y are the state of input and output vectors, A, B and C are matrixes, of orders $mxm, mx1, 1xm$, and α is called commensurate of fractional order.

According to (Matignon, 1998) the FOS $D^{\alpha}x = Ax$ is asymptotically stable, if the condition

$$|\arg(\mathrm{eig}(\mathrm{A}))| > \alpha\frac{\pi}{2} \text{ for } 0 < \alpha < 2 \qquad \textbf{(2.23)}$$

is met, where $(eig(A))$ is the "eigenvalues of matrix A". Note that $eig(A)$ are the zeros of the characteristic polynomial

$$\mathrm{d}(\mathrm{p}) = \det(\mathrm{pI} - \mathrm{A}) = \sum_{\mathrm{i}=0}^{\mathrm{m}} \mathrm{d_i}\ (\mathrm{s}^{\propto})^{\mathrm{i}}, \text{where } \mathrm{p} = \mathrm{s}^{\alpha}. \qquad (\mathbf{2.24})$$

Hence, the characteristic polynomial is a commensurate polynomial in s with the common power of α. Therefore, the stability criterion of Matignon is valid for any FO system having a commensurate characteristic polynomial.

Note that the transfer function of the system defined in Eqs. (2.21) and (2.22) is

$$\mathrm{TF} = \frac{\mathrm{Y(s)}}{\mathrm{X(s)}} = \mathrm{C}(\mathrm{s}^{\alpha}\mathrm{I} - \mathrm{A})^{-1}\mathrm{D} = \frac{\mathrm{CAdj}(\mathrm{s}^{\alpha}\mathrm{I} - \mathrm{A})\mathrm{D}}{\det(\mathrm{s}^{\alpha}\mathrm{I} - \mathrm{A})}. \qquad (\mathbf{2.25})$$

And hence the characteristic equation in Eq. (2.20) is said in commensurate form with

$$\sum_{i=0}^{m} a_i s^{\propto_i} \sum_{i=0}^{n} d_i \ (s^{\alpha})^i. \qquad (\mathbf{2.26})$$

Hence, power in Eq. (2.20) is a multiple of some common power α , that is $\propto_i = \alpha_i, i = 0,1,\cdots,m.$

The regions of the system stability and instability of the FOS for the values of $0 < \alpha \leq 1$ and $1 < \alpha < 2$ on the complex frequency plane $s = \sigma + j\omega$ are demonstrated in (Figs. 2.1 and 2.2).

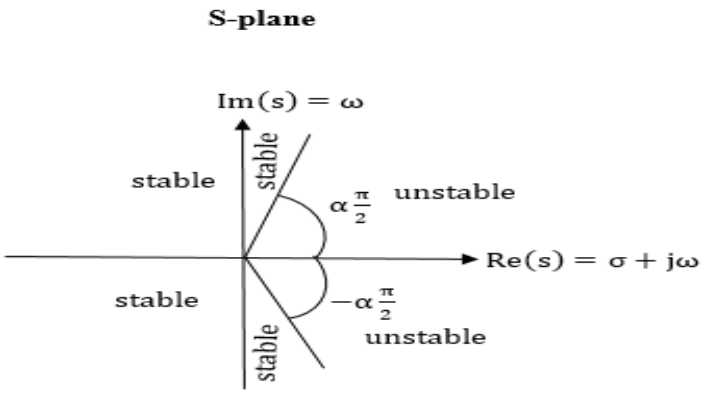

Figure 2. 1. Stability regions of fractional order LTI system with order $0 < \alpha \leq 1$

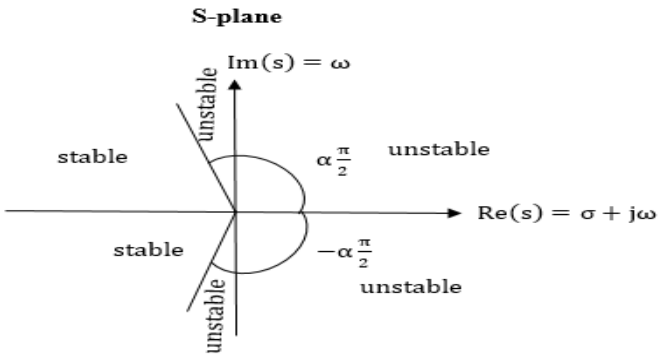

Figure 2. 2. Stability regions of fractional order LTI system with order $1 < \alpha < 2$

When applied to the characteristic Eq. (2.24) of the SISO FOPID control system, the characteristic polynomial can be obtained as the numerator polynomial of the characteristic Eq. (2.24).

3. FRACTIONAL ORDER PID CONTROL SYSTEM DESIGN

In this chapter, the FOPID control system structure is reconsidered again and the design specifications of the FOPID controller are outlined.

3.1. Control System Structure

A Single-input single-output (SISO) general form of fractional order control system is a generalization of the structure given in Fig. 1.1 as seen in Fig. 3.1.

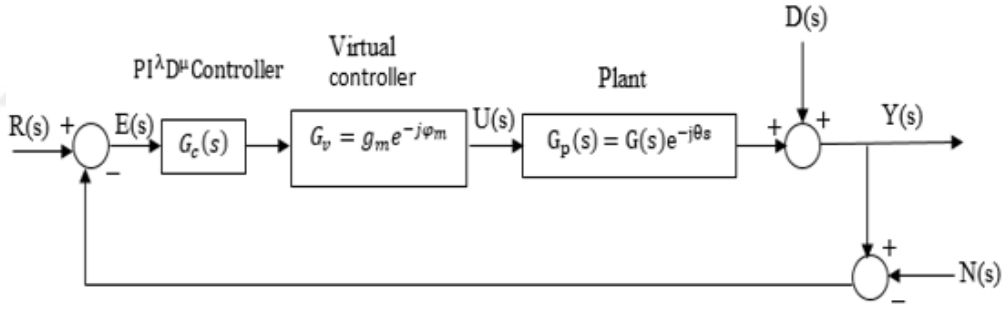

Figure 3. 1. Basic structure of SISO fractional-order control system

In this figure, $Y(s)$ represents the output of the system, $U(s)$ is the controller's output signal, $R(s)$ is the reference or the preferred input, $E(s)$ is the error between the reference input and the output. $G_c(s)$ is the fractional order PID controller's transfer function and $G_p(s)$ is the transfer function of the controlled system. $D(s)$ and $N(s)$ represent the output disturbance and measurement noise, respectively. This type of systems can be controlled both integer and/or fractional orders (arbitrary order systems) of the controllers.

In this figure

$$G_v = g_m e^{-j\varphi_m} \quad \textbf{(3.1)}$$

is defined as a virtual gain; it is not actually present and it is included to gain some relative stability requirements gain margin g_m and phase margin φ_m that will be defined in the

sequel (see Eqs. (3.14) and (3.15)). It is the transfer function of the virtual compensator which is also called gain-phase margin tester, GPMT (Cokmez et al, 2018; Hamamci, 2007). Therefore, in the following discussions it should be taken as an identity ($G_v = 1$), otherwise stated.

Considering the unity feedback system in Fig. 3.1, the transfer function of the FOPID system controller $G_c(s)$ is in the form bellow

$$\mathrm{G_c} = \frac{\mathrm{U(s)}}{\mathrm{E(s)}} = \mathrm{K_p} + \frac{\mathrm{K_i}}{\mathrm{s^{\lambda}}} + \mathrm{K_d s^{\mu}} = \frac{\mathrm{K_d S^{\lambda+\mu} + K_p S^{\lambda} + K_i}}{\mathrm{S^{\lambda}}} \qquad \textbf{(3.2)}$$

where μ and λ are the fractional orders of derivative and integrals respectively. The transfer function of the controlled systems is defined as

$$\mathrm{G_p(s) = G(s)e^{-\theta s}} = \frac{\mathrm{N(s)}}{\mathrm{D(s)}}\mathrm{e^{-\theta s}} = \frac{\sum_{j=0}^{n} \mathrm{b_j\ S^{\beta_j}}}{\sum_{i=0}^{m} \mathrm{a_i\ S^{\propto_i}}}\mathrm{e^{-\theta s}}, \qquad (\mathbf{3.3})$$

or it can be represent as

$$\left(\sum_{i=0}^{m} \mathrm{a_i\ D^{\alpha_i}}\right)\mathrm{y(t)} = \left(\sum_{j=0}^{n} \mathrm{b_j\ D^{\beta_j}}\right)\mathrm{u(t-\theta)}. \qquad (\mathbf{3.4})$$

The output of the control system is given as

$$\mathrm{Y(s)} = \frac{\mathrm{G_c\,(s)G_v\,G_p(s)}}{1+\mathrm{G_c\,(s)G_v\,G_p(s)}}\mathrm{R(s)} + \frac{\mathrm{G_c\,(s)G_v\,G_p(s)}}{1+\mathrm{G_c\,(s)G_v\,G_p(s)}}\mathrm{N(s)} + \frac{1}{1+\mathrm{G_c\,(s)G_v\,G_p(s)}}\mathrm{D(s)}$$
$$= \mathrm{T_R(s)R(s) + T_N(s)N(s) + T_D(s)D(s)} \qquad (\mathbf{3.5})$$

Above, $T_R(s), T_N(s), T_D(s)$ are the transfer functions between the input reference, the noise signal, the disturbance signal and the controlled output of the plant.

A LTI system to be a stable system all the zeros of the denominator that is the roots of the characteristic equation

$$1 + \mathrm{G_c\,(s)G_v\,G_p(s)} = 0 \qquad \textbf{(3.6)}$$

have to be in the left half plan (LHP).

3.2. Relative Stability of FOPID Control System

If the characteristic Eq. (3.5) does not lead to a commensurate characteristic polynomial as in Eq. (2.24), which is usually the case, then the stability test therein cannot be applied. Therefore, another stability test is needed for FOPID control system. In this case, to check the system stability in frequency domain, we first convert the s-plane into the complex plane $G_c\,(j\omega)G_p(j\omega)$ and the conversion is done considering the open loop transfer function $G_c\,(j\omega)G_p(j\omega)$ of the system. Through the conversion, all the poles of the denominator of the transfer functions in Eq. (3.4) are mapped from s-plane into a "critical point" (-1,0j) in the complex plane of $G_c\,(j\omega)G_p(j\omega)$.

The transformation of the s-plane into a complex plane $G_c\,(j\omega)G_p(j\omega)$ is conform, such that, the path and position of all the points in s-plane is conserved in the complex plane $G_c\,(j\omega)G_p(j\omega)$. Nyquist frequency characteristics of frequency examination techniques of stability and the consumption of its principle are designated in (Petras et al, 2000).

This test is known as the Nyquist criteria and is considered in this section. When passing from the left-hand s-plane to the right-hand s-plane, the roots of the characteristic Eq. (2.24) become purely imaginary and this equation takes the form

$$\mathrm{G_c(j\omega)G_p\,(j\omega)} = -1 \qquad \textbf{(3.7)}$$

which defines a border on the parameter space between the stable and unstable states, the parameters are implicit and being those of the transfer functions $G_c(s)$ and $C_p\,(s)$.This case is better illustrated by the unity gain and -180^o phase of the open loop gain function $G_c(j\omega)C_p\,(j\omega)$; in other words

$$\mathrm{M(\omega) = \left|G_c(j\omega)G_p\,(j\omega)\right| = 1} \qquad \textbf{(3.8)}$$

$$\mathrm{\emptyset(\omega) = Arg\left[G_c(j\omega)G_p\,(j\omega)\right] = 180^o.} \qquad \textbf{(3.9)}$$

The Nyquist plot of the open loop gain $G_c(j\omega)G_p\,(j\omega)$ is obtained as the plot on the complex $G_c(j\omega)G_p\,(j\omega)$ plane for $\omega = [0, \infty)$, and the typical plots are shown in fig. 3.2

The critical point which enters the system into the unstable state is $(-1, 0)$. Two plots one indicating an unstable closed-loop system (CLS) and the other is a stable CLS are also indicated in Fig. 3..2 by line styles '---' and '-.-.-.' respectively. The gain crossover frequency ω_{gc} and the phase crossover frequency ω_{pc} are defined by

$$\mathrm{M}(\omega_{\mathrm{gc}}) = \left|\mathrm{G_c}(\mathrm{j}\omega_{\mathrm{gc}})\mathrm{G_p}\,(\mathrm{j}\omega_{\mathrm{gc}})\right| = 1\,. \tag{3.10}$$

$$\emptyset(\mathrm{j}\omega_{\mathrm{pc}}) = \mathrm{Arg}\left[\mathrm{G_c}(\mathrm{j}\omega)\mathrm{G_p}\,(\mathrm{j}\omega)\right] = 180^{\mathrm{o}}\,, \tag{3.11}$$

respectively. The gain cross-over point (GCOP) and the phase cross-over point (PCOP) are defined in polar coordinates as

$$\mathrm{GCOP}:\ \left(-\tfrac{1}{\mathrm{g_m}}, \pi\right), \tag{3.12}$$

$$\mathrm{PCOP}:\ (1, \pi + \varphi_{\mathrm{m}}), \tag{3.13}$$

respectively; where

$$\mathrm{g_m} = -\frac{1}{\mathrm{G_g}(\mathrm{j}\omega_{\mathrm{pc}})\mathrm{C_c}\,(\mathrm{j}\omega_{\mathrm{pc}})},\quad \mathrm{GM} = 20\log(\mathrm{g_m})\ \text{in dB} \tag{3.14}$$

$$\varphi_{\mathrm{m}} = \pi - \arg\left[\mathrm{G_g}(\mathrm{j}\omega_{\mathrm{pc}})\mathrm{C_c}\,(\mathrm{j}\omega_{\mathrm{pc}})\right],\qquad \mathrm{PM} = \frac{180^{\mathrm{o}}}{\pi}\varphi_{\mathrm{m}}\ \text{ in degrees} \tag{3.15}$$

are defined as the gain margin and phase margin, respectively. Note that the gain margin and the phase margin are expressed in decibels and degrees respectively and denoted GM and PM, specifying the relative stability of the CLS. In other words, greater GM results with a PCOP far away from the critical instability point $(-1, 0)$ hence with a more stable CLS. Similarly, greater PM results with a GCOP far away from the critical instability point $(-1, 0)$ hence with a more stable CLS. A gain margin $> 20\ dB$ and a phase margin $> 60^{o}$ results with a sufficiently stable CLSs. Therefore, GM and PM are very important concepts in designing integer order and fractional order controllers for control systems.

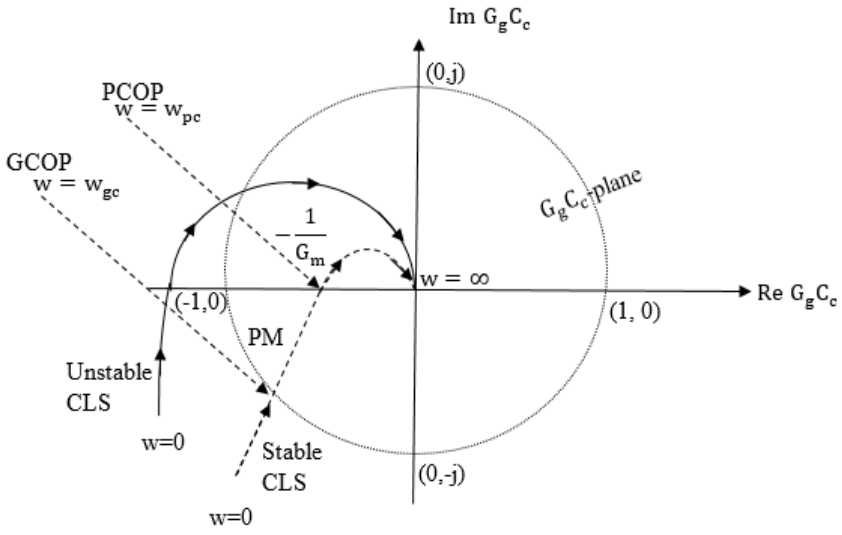

Figure 3. 2. Typical Nyquist plot of the open loop gain $G_g(j\omega)C_c\,(j\omega)$

Gain and phase margins serve as important measures of robustness as well. It is known that PM is related to damping of the system and therefore can also serve as a performance measure (Monje et al, 2008; Franklin et al, 1998).

3.3. Frequency Domain Methods of FOPID Controller Design

Traditional PID control is a standard feedback mechanism control loop, commonly used in many industrial applications. This PID controller tries to accurate the error, which is the difference between the reference measured variable and the required output value, by computing and fixing the error for the corrective achievement that can regulate the procedure accordingly.

The transfer function of the traditional integer-order PID controller is given in Eq. (1.8). Three different parameters have involved the standard PID controllers: (K_p, K_i, K_d) which are the proportional, integral and the derivative gain constants of the controllers respectively.

The proportional gain constant is used to determine the present error response, the integral gain constant is used to determine the previous latest errors based on the responses and the derivative gain constant is used to determine the response of the system to the degree at which the error had been varying.

Different control elements such as the heat control, automatic voltage regulator, power supply controlling and many other control elements use these combined three control elements to adjust and control their processes system of PID controller. Generally, the functional process of real objects are considered. Though the FOSs are very low, commonly the integer-order system's approximation might have some significant variations between the real systems and their mathematical styles.

Due to the luck of fractional deferential equation's solutions (FDEs), integer-order prototypes are used. PID controller is one of the leading industrial system controllers used today, and hence are the things of putting very strong effort to develop the quality of PID control systems and the robustness of the system.

So using fractional order PID is one of the most important possibilities to progress the traditional PID controllers and it is denoted or called by $PI^{\lambda}D^{\mu}$. FOPID was presented in (Kaczorek, 2008; El-Sayed et al, 2007; Podlubny, 1999).

The general form of FOPID controller is given in Eq. (1.12), and there are two surplus parameters compared to the conventional PID controller equation given in Eq. (1.8).

To design a FOPID controller in the form of Eq. (1.12), there are five different parameters to consider $(K_p, K_i, K_d, \lambda, \mu)$ in order to turn, and these five different parameters increases the flexibility of succeeding the current preferred requirements, "for example controlling the steady state errors, margins of gain and phase, or even the system performances and robustness". However, these also increase the system complexity anyway. So, the trail is to develop a feasible and reliable FOPID controller that behaves and meets the identical system design requirements (necessities) and performance, but has less parameter numbers. And the most important point here is to find out for suitable and achievable estimation to the integral and derivative operators $(\lambda,\ \mu)$.

Numerous efforts to discover an optimal set for $PI^{\lambda}D^{\mu}$ controller's five parameters have been studied, so as to accomplish predefined desires of the system (El-Khazali, 2013; Biswas et al, 2009). For designing $PI^{\lambda}D^{\mu}$ controllers, Ziegler-Nichols parameters tuning rules were stated in (Valério and Da Costa, 2004). Also some other new methods for the tuning parameters of the $PI^{\lambda}D^{\mu}$ controllers have been stated recently in (Veronesi and Visioli, 2010; Maiti et al, 2008). Reference (El-Khazali, 2013) suggested assuming that

$\lambda = \mu$ and $\tau_i = \tau_d$, in order to simplify the design procedure of the $PI^{\lambda}D^{\mu}$ controller, and then Eq. (1.12) can be modified as

$$G_c(s) = K_p\left(1 + \frac{1}{\tau_i S^{\mu}} + \tau_i S^{\mu}\right), \quad \textbf{(3.16)}$$

or even modify more using biquadratic formulation

$$G_c(s) = K_p\left(2 + \frac{1}{\tau_i S^{\mu}} + \tau_i S^{\mu}\right) = K_c \frac{(1+\tau_i S^{\mu})^2}{S^{\mu}} \text{ ; where } K_c = \frac{K_p}{\tau_i}. \quad \textbf{(3.17)}$$

Apparently, the five parameters in Eq. (3.2) is compacted into only three parameters that have to be select carefully to control and meet the requirements of the system design. And to find the integral time constant (τ_i) and the fractional order (μ), (El-Khazali, 2013) uses the following equations.

$$\mu = \frac{-\pi + \varphi_m - \theta_p}{\frac{\pi}{2}}, K_c = \frac{1}{g_p g_m}, \quad \textbf{(3.18)}$$

$$\tau_i = \left\{\frac{\tan\left(\frac{\varphi_c}{2}\right) + \tan\left(\frac{2+\mu}{\pi/4}\right)}{\tan\left(\frac{\varphi_c}{2}\right) - \tan\left(\frac{2+\mu}{\pi/4}\right)}\right\} \text{ ; for } \varphi_c \neq \left(\frac{2+\pi}{\pi/8}\right), \quad \textbf{(3.19)}$$

$$\varphi_c = 2\tan^{-1}\left\{\frac{(\tau_i+1) + \tan\left(\frac{2+\mu}{\pi/4}\right)}{\tau_i - 1}\right\} \text{ ; for } \tau_i \neq 1, \quad \textbf{(3.20)}$$

where φ_m and g_m are the preferred phase and gain margins, θ_p and g_p are the phase and the gain margins of the uncontrolled system, and φ_c is the controller's phase-angle.

4. 3D METHOD OF DESIGNING FOPID CONTROLLER

In this thesis, a graphical method is developed to tune the gain parameters K_p, K_i, K_d of the FOPID controller knowing the fractional orders λ and μ . The method gives a graphical view of the acceptable control parameters satisfying the specified requirements on the 3- dimensional Euclid space $(K_p, K_i, K_d) \in R^3$. Although some of them have been mentioned in the previous chapters of the thesis, the specifications considered are summarized in the following subsection for the sake of completeness and compactness of the presented design method. The method has not been implied before. Also 3-dimensinal plots, their mathematical and programming details as well as 3-D examples are not studied thoroughly in the literature.

4.1. Design Specifications

Frequency domain design specifications for robust FOPID tuning frequency domain design (Das et al, 2011) of FOPID controllers was proposed by (Monje et al, 2008) based on a constrained optimization problem, i.e. if $G_p(s)$ given in Eq. (3.3) is the model of the process plant, then the objective is to find a controller $G_c\ (s)$ as given in Eq. (3.2), so that the open loop system would meet the following design specifications:

(a) Phase margin specification: For sufficiently good relative stability phase margin should be greater or equal to some pre-assigned value. Attaining a preferred phase margin PM (see Eq. 3.15) at the gain-crossover frequency w_{gc} (see Eq. 3.9). Equations are repeated below for the compactness of the design specifications

$$\varphi_m = \pi - \arg\left[G_c(j\omega_{gc})G_p(j\omega_{gc})\right], \quad \textbf{(4.1)}$$

$$M(\omega_{gc}) = \left|G_c(j\omega_{gc})G_p(j\omega_{gc})\right| = 1. \quad \textbf{(4.2)}$$

(b) Gain margin specification: Sustaining a preferred gain-margin GM (see Eq. 3.14) of the closed-loop system at the phase crossover frequency w_{pc} (see Eq. 3.10) of the open loo system. Equations are repeated below for the compactness of the design specifications

$$g_m = -\frac{1}{G_g(j\omega_{pc})C_c(j\omega_{pc})} \quad (\mathbf{4.3})$$

$$\emptyset(j\omega_{pc}) = \mathrm{Arg}[G_g(j\omega_{pc})C_c(j\omega_{pc})]. \quad \mathbf{(4.4)}$$

(c) Robustness to gain variation (Iso-damping): The phase of the open loop system must be flat at ω_{gc} (Chen et al, 2003). This condition given in Eq. (4.5) forces the phase of the open loop system to be flat at ω_{gc} and almost constant in its neighborhood ($\psi_{spec} \leq 0$, decreasing ψ_{spec} increases relative stability). The system is more robust to gain changes and the overshoot of the response is almost constant within a gain range, which is known as iso-damping of time response.

$$\frac{d}{d\omega}\mathrm{Arg}[G_c(j\omega)G_p(j\omega)]\big|_{\omega=\omega_{gc}} = -\psi_{spec} \text{ (usually 0).} \quad \mathbf{(4.5)}$$

(d) Output disturbance rejection: A constraint on the disturbance transfer function $T_D(s)$ in Eq. (3.5) with $G_v = 1$, can be set to prevent the low frequency disturbance by setting (Monje et al, 2008; Das et al, 2011)

$$\left|T_D(j\omega) = \frac{1}{1+G_c(j\omega)G_p(j\omega)}\right|_{\omega\leq\omega_d} \leq B_d, \quad \mathbf{(4.6)}$$

where B_d is an upper limit for the noise gain for frequencies $\omega \leq \omega_d$. B_d is the load disturbance suppression for frequencies $\omega \leq \omega_d$ (Das et al, 2011).

(e) High frequency noise rejection: A constraint on the noise transfer function $T_N(s)$ in Eq. (3.5) with $G_v = 1$ (also known as the complementary sensitivity function or noise attenuation requirement (Das et al, 2011)), can be set to prevent the interference of high frequency noise by setting

$$\left|T_N(j\omega) = \frac{G_c(j\omega)G_p(j\omega)}{1+G_c(j\omega)G_p(j\omega)}\right|_{\omega\geq\omega_n} \leq C_n, \quad \mathbf{(4.7)}$$

where C_n is a lower limit on the complementary sensitivity function for frequencies $\omega \geq \omega_n$ (Das et al, 2011; Monje et al, 2008).

The condition (b) is not included as a design specification in (Monje et al, 2008). Due to its importance from relative stability point of view and to guarantee a stable control system, it is included in design requirements in this thesis. Further, although steady-state error cancellation is included in (Monje et al, 2008), the fractional integration $s^{-\lambda}$ in the controller is an efficient term to cancel the steady-state error so the steady-state error specification is automatically fulfilled, and this specification is null and not included in the above specification list.

4.2. Formulation of Design Specifications

To achieve the required performance parameters $\varphi_m, g_m, \omega_{gc}, \psi_{spec}, \omega_n, C_n, \omega_d, B_d$ defined in the previous subsection, the values that controller gains K_p, K_i, K_d can take will be discussed graphically in this section by using 3D plots in the space $(K_p, K_i, K_d) \in R^3$. The plant transfer function is assumed to be given as a fractional order rational function with a time delay as in the form of Eq. (3.3); the fractional order integrator and differentiator control orders λ and μ are assumed to be known as well; λ and μ are either known or can be found using by the existing methods in the literature (for example see the references (Biswas et al, 2009), (Maiti et al, 2008), (Zamani et al, 2009) (El-Khazali, 2013), (Valério and Da Costa, 2004), (Veronesi and Visioli, 2010)).

4.2.1. Stability boundaries

To find the stability boundaries (Cokmez et al, 2018; Hamamci, 2007; Tan et al, 2006) for achieving the specified phase and gain margins defined by items (a) and (b) in Section 4.1, consider Eq. (3.6) together with Eqs. (3.1), (3.2) and (3.3).

Real root boundary (RRB) is found by letting $s = 0$ in Eq. (3.6) which leads to

$$\mathrm{K_i} = 0. \tag{4.8}$$

Hence, RRB is a plane perpendicular to $K_p - K_i$ plane in $(K_p, K_i, K_d) = R^3$.

Complex root boundary (CRB) is obtained by $s = j\omega$ in Eq. (3.6); this leads to the Eqs. (3.8) and (3.9).

Using the expressions (3.2), (3.3), (4.8) in (3.8) we obtain

$$K_p^2\omega^{2\lambda} + K_d^2\omega^{2(\lambda+\mu)} + K_i^2 + 2K_pK_d\omega^{2\lambda+\mu}\cos(0.5\pi\mu) + 2K_pK_i\omega^{\lambda}\cos(0.5\pi\lambda)$$

$$+2K_dK_i\omega^{\lambda+\mu}\cos\big(0.5\pi(\lambda+\mu)\big) = \frac{\omega^{2\lambda}}{N^2}\text{, where} \quad \textbf{(4.9)}$$

$$G_vG_p(j\omega) = Ne^{j\gamma}. \quad \textbf{(4.10)}$$

N and γ can be found from Eqs. (3.1) and (3.3) as follows:

$$N = g_m\left[\frac{[\sum_{k=0}^{n} b_k\cos(0.5\pi\beta_k)]^2 + [\sum_{k=0}^{n} b_k\sin(0.5\pi\beta_k)]^2}{[\sum_{r=0}^{n} a_r\cos(0.5\pi\alpha_r)]^2 + [\sum_{r=0}^{n} a_r\sin(0.5\pi\alpha_r)]^2}\right]^{1/2} \quad (\mathbf{4.11})$$

$$\gamma = -\varphi_m + \arctan\frac{\sum_{k=0}^{n} b_k\sin(0.5\pi\beta_k)}{\sum_{k=0}^{n} b_k\cos(0.5\pi\beta_k)} - \arctan\frac{\sum_{r=0}^{n} a_r\sin(0.5\pi\alpha_r)}{\sum_{r=0}^{n} a_r\cos(0.5\pi\alpha_r)} - \theta\omega. \quad (\mathbf{4.12})$$

Using the expressions (3.1), (3.2), and (3.3) in (3.9), we obtain

$$K_p\omega^{\lambda}\sin(\gamma) - K_i\sin(0.5\pi\lambda - \gamma) + K_d\omega^{\lambda+\mu}\sin(0.5\pi\mu + \gamma) = 0. \quad \textbf{(4.13)}$$

Drawing K_i from Eq. (4.13) and inserting in Eq. (4.9) and arranging after long calculations Eq. (4.9) takes the simpler form

$$K_p\omega^{\lambda}\sin(0.5\pi\lambda) + K_d\omega^{\lambda+\mu}\sin\big(0.5\pi(\lambda+\mu)\big) = \mp\frac{\omega^{\lambda}}{N}\sin(0.5\pi\lambda - \gamma). \quad \textbf{(4.14)}$$

As the summary of the derivation, CRB defined by Eqs. (3.8) and (3.9) lead to the compact form

$$\begin{bmatrix} \sin\left(\frac{\pi}{2}\lambda\right) & 0 & \omega^{\mu}\sin\left[\frac{\pi}{2}(\lambda+\mu)\right] \\ \sin(\gamma) & -\omega^{-\lambda}\sin\left(\frac{\pi}{2}\lambda - \gamma\right) & \omega^{\mu}\sin\left[\frac{\pi}{2}(\lambda+\gamma)\right] \end{bmatrix}\begin{bmatrix} K_p \\ K_i \\ K_d \end{bmatrix} = \begin{bmatrix} \mp\frac{\sin\left(\frac{\pi}{2}\lambda-\gamma\right)}{N} \\ 0 \end{bmatrix}.$$

(4.15)

Using some matrix manipulations the above matrix equation can be extended as

$$\begin{bmatrix} \omega^{\lambda}\sin\left(\frac{\pi}{2}\lambda\right) & 0 & \omega^{\lambda+\mu}\sin\left[\frac{\pi}{2}(\lambda+\mu)\right] \\ 0 & \sin\left(\frac{\pi}{2}\lambda\right) & -\omega^{\lambda+\mu}\sin\left(\frac{\pi}{2}\mu\right) \\ \omega^{\lambda}\sin\left(\frac{\pi}{2}\mu\right) & \sin\left[\frac{\pi}{2}(\lambda+\mu)\right] & 0 \end{bmatrix}\begin{bmatrix} K_p \\ K_i \\ K_d \end{bmatrix} = \mp\frac{\omega^{\lambda}}{N}\begin{bmatrix} \frac{\sin\left(\frac{\pi}{2}\lambda-\gamma\right)}{N} \\ \sin(\gamma) \\ \sin\left(\frac{\pi}{2}\lambda+\gamma\right) \end{bmatrix}.$$

(4.16)

In this form, only any 2 of the equations are linearly independent at a time and the remaining is linearly dependent on these two. In 3-dimensional Euclid space $R^3 = (K_p, K_i, K_d)$ Eq. (4.15) defines a surface as the parameter ω changes from 0 to ∞. This surface separates the stable and unstable regions with $G_v = g_m e^{-j\varphi_m}$ present in the control loop; further if $G_v = 1$ the stable region guaranties the stability with the required gain and phase margins.

Infinite root boundary (IRB) which results when $\omega \to \infty$ does not exists for the control system applications (Cokmez et al, 2018; Hamamci, 2007).

The illustration of finding RRB, CRB, IRB stability boundaries and the programming details will be given in Chapter 5.

4.2.2. Phase flatness surface and flatness curve

First, the gain crossover frequency condition in Eq. (4.2) is used together with Eqs. (3.2) and (3.3) defining G_c and G_p to obtain Eq. (3.8) with N given in Eq. (4.11) and with $g_m = 1$. Second, the phase flatness condition in Eq. (4.5) is used together with Eq. (3.2) and (3.3) defining G_c and G_p (see Eq. (4.18) given below). Combining these two conditions, the equations describing constant phase flatness surface in 3-dimensional space are obtained as:

$$\mathrm{K_p^2}\omega^{2\lambda} + \mathrm{K_d^2}\omega^{2(\lambda+\mu)} + \mathrm{K_i^2} + 2\mathrm{K_p K_d}\omega^{2\lambda+\mu}\cos(0.5\pi\mu) + 2\mathrm{K_p K_i}\omega^{\lambda}\cos(0.5\pi\lambda) + 2\mathrm{K_d K_i}\omega^{\lambda+\mu}\cos\big(0.5\pi(\lambda+\mu)\big) = \frac{\omega^{2\lambda}}{\mathrm{N^2}}, \quad \textbf{(4.17)}$$

$$\mathrm{K_p K_i}\lambda\sin(0.5\pi\lambda) + \mathrm{K_p K_d}\omega^{\lambda+\mu}\mu\sin(0.5\pi\mu) + \mathrm{K_i K_d}(\lambda+\mu)\omega^{\mu}\sin[0.5\pi(\lambda+\mu)] = \frac{\omega^{\lambda+\mu}}{\mathrm{N^2}}\Big(\theta - \psi_{\mathrm{spec}} - \frac{\mathrm{d}\beta}{\mathrm{d}\omega}\Big), \quad \textbf{(4.18)}$$

where $N, \beta, \gamma, \frac{d\beta}{d\omega}$ are

$$\mathrm{N} = \left[\frac{[\sum_{k=0}^{n} \mathrm{b_k}\cos(0.5\pi\beta_k)]^2 + [\sum_{k=0}^{n} \mathrm{b_k}\sin(0.5\pi\beta_k)]^2}{[\sum_{r=0}^{n} \mathrm{a_r}\cos(0.5\pi\alpha_r)]^2 + [\sum_{r=0}^{n} \mathrm{a_r}\sin(0.5\pi\alpha_r)]^2}\right]^{1/2}, \quad (\mathbf{4.19})$$

$$\beta = \mathrm{Arctan}\frac{\sum_{k=0}^{n} \mathrm{b_k}\sin(0.5\pi\beta_k)}{\sum_{k=0}^{n} \mathrm{b_k}\cos(0.5\pi\beta_k)} - \arctan\frac{\sum_{r=0}^{n} \mathrm{a_r}\sin(0.5\pi\alpha_r)}{\sum_{r=0}^{n} \mathrm{a_r}\cos(0.5\pi\alpha_r)}, \quad (\mathbf{4.20})$$

$$\gamma = \beta - \theta\omega\,, \tag{4.21}$$

$$\frac{d\beta}{d\omega} = \frac{\omega^{-1}\sum_{k=1}^{n-1}\left[\sum_{h=k+1}^{n} b_k b_h \omega^{\beta_k+\beta_h}(\beta_k-\beta_h)\sin[0.5\pi(\beta_k-\beta_h)]\right]}{\sum_{k=1}^{n} b_k^2\omega^{2\beta_k} + 2\sum_{k=1}^{n-1}\left[\sum_{h=k+1}^{n} b_k b_h \omega^{\beta_k+\beta_h}\cos[0.5\pi(\beta_k-\beta_h)]\right]}$$

$$-\frac{\omega^{-1}\sum_{r=1}^{m-1}\left[\sum_{h=r+1}^{m} a_r a_h \omega^{\alpha_r+\alpha_h}(\alpha_r-\alpha_h)\sin[0.5\pi(\alpha_r-\alpha_h)]\right]}{\sum_{r=1}^{m} a_r^2\omega^{2\alpha_r} + 2\sum_{r=1}^{m-1}\left[\sum_{h=r+1}^{m} a_r a_h \omega^{\alpha_r+\alpha_h}\cos[0.5\pi(\alpha_r-\alpha_h)]\right]}\,. \tag{4.22}$$

On the face flatness surface $\psi_f = -\psi_{spec}$, the value of the face flatness in Eq. (4.5) is exactly satisfied, that is $\psi_f = -\psi_{spec}$. On one side of this surface the flatness is smaller than the value specified by this equation, and on the other side greater. In the design of the controller, any point (K_p, K_i, K_d) chosen on this surface or the greater side will fulfill the requirement

$$\frac{d}{d\omega}\mathrm{Arg}\left[G_c(j\omega)G_p(j\omega)\right]\Big|_{\omega=\omega_{gc}} \geq -\psi_{spec} \ (\text{usually } 0). \tag{4.23}$$

If the gain cross over frequency ω_{gc} is given, then Eqs. (4.17) and (4.18) define a curve in the 3-dimensional (K_p, K_i, K_d) space where Eqs. (4.19), (4.20) and (4.21) are evaluated at $\omega = \omega_{gc}$. This curve is defined as the flatness curve on which Eq. (4.5) is satisfied.

4.2.3. Disturbance rejection surface

Using Eqs. (3.2) and (3.3) for $G_c\,(s = j\omega_d)$ and $G_p(s = j\omega_d)$, respectively, the equation of disturbance rejection surface is obtained from Eq. (4.6) by taking the equality sign as

$$\left[K_p\omega_d^{\lambda} + K_i\cos(0.5\pi\lambda) + K_d\omega_d^{\lambda+\mu}\cos(0.5\pi\mu) + \frac{\omega_d^{\lambda}}{N}\cos(\gamma)\right]^2$$
$$+\left[K_i\sin(0.5\pi\lambda) - K_d\sin(0.5\pi\mu) + \frac{\omega_d^{\lambda}}{N}\sin(\gamma)\right]^2 = \frac{\omega_d^{2\lambda}}{N^2B_d^2}. \tag{4.24}$$

Or equivalently,

$$\left[P + I\cos(0.5\pi\lambda) + D\cos(0.5\pi\mu) + \frac{\omega_d^{\lambda}}{N}\cos(\gamma)\right]^2$$
$$+\left[I\sin(0.5\pi\lambda) - D\sin(0.5\pi\mu) + \frac{\omega_d^{\lambda}}{N}\cos(\gamma)\right]^2 = \frac{\omega_d^{2\lambda}}{N^2B_d^2} \tag{4.25}$$

where $G_p(j\omega_d) = Ne^{j\gamma};\ N, \gamma$ are

$$\mathrm{N} = \left[\frac{\left[\sum_{k=0}^{n} b_k \omega_d^{\beta_k} \cos(0.5\pi\beta_k)\right]^2 + \left[\sum_{k=0}^{n} b_k\, \omega_d^{\beta_k} \sin(0.5\pi\beta_k)\right]^2}{\left[\sum_{r=0}^{n} a_r\, \omega_d^{\alpha_r} \cos(0.5\pi\alpha_r)\right]^2 + \left[\sum_{r=0}^{n} a_r\, \omega_d^{\alpha_r} \sin(0.5\pi\alpha_r)\right]^2}\right]^{1/2} \quad (\mathbf{4.26})$$

$$\gamma = \mathrm{Arctan}\frac{\sum_{k=0}^{n} b_k\, \omega_d^{\beta_k} \sin(0.5\pi\beta_k)}{\sum_{k=0}^{n} b_k \omega_d^{\beta_k} \cos(0.5\pi\beta_k)} - \arctan\frac{\sum_{r=0}^{n} a_r\, \omega_d^{\alpha_r} \sin(0.5\pi\alpha_r)}{\sum_{r=0}^{n} a_r\, \omega_d^{\alpha_r} \cos(0.5\pi\alpha_r)} - \theta\omega_d, \quad (\mathbf{4.27})$$

$$\mathrm{P} = \mathrm{K_p}\omega_d^{\lambda}, \mathrm{I} = \mathrm{K_i}, \mathrm{D} = \mathrm{K_d}\omega_d^{\lambda+\mu}. \quad \textbf{(4.28)}$$

Output disturbance rejection specification is satisfied on the side

$$[\cdot]^2 + [\cdot]^2 \geq \frac{\omega_d^{2\lambda}}{N^2 B_d^2},\ \text{for all } \omega \leq \omega_d\ , \quad \textbf{(4.29)}$$

of this surface where the term in the parenthesis represent the left-hand sides of Eqs. (4.24) and (4.25) with N and γ taken as in Eq. (4.26) and Eq. (4.27), respectively.

4.2.4. High frequency noise rejection surface

High frequency noise rejection condition in Eq. (4.7) together with Eqs. (3.2) and (3.3) for $G_c\,(s = j\omega_n)$ and $G_p(s = j\omega_{dn})$, respectively, yield

$$\frac{C_n^2 - 1}{C_n^2}[P^2 + I^2 + D^2 + 2PI\cos(0.5\pi\lambda) + 2PD\cos(0.5\pi\mu) + 2IDcos\{0.5\pi(\lambda + \mu)\}]$$

$$+\frac{2\omega_n^{\lambda}}{N}[Pcos(\gamma) + I\cos(0.5\pi\lambda - \gamma) + Dcos(0.5\pi\mu + \gamma] + \frac{\omega^{2\lambda}}{N^2} \geq 0. \quad \textbf{(4.30)}$$

Or, assuming $|C_n| \leq 1$ which is usually the case,

$$[P^2 + I^2 + D^2 + 2PI\cos(0.5\pi\lambda) + 2PD\cos(0.5\pi\mu) + 2IDcos\{0.5\pi(\lambda + \mu)\}]$$

$$+\frac{2\omega_n^{\lambda}C_n^2}{N(C_n^2-1)}[Pcos(\gamma) + I\cos(0.5\pi\lambda - \gamma) + Dcos(0.5\pi\mu + \gamma] + \frac{\omega_n^{2\lambda}C_n^2}{N^2(C_n^2-1)} \leq 0. \quad \textbf{(4.31)}$$

In Eqs. (4.30) and (4.31) $G_p(j\omega_n) = Ne^{j\gamma};\ N, \gamma, P, I, D$ are

$$\mathrm{N} = \left[\frac{\left[\sum_{k=0}^{n} b_k \omega_n^{\beta_k} \cos(0.5\pi\beta_k)\right]^2 + \left[\sum_{k=0}^{n} b_k\, \omega_n^{\beta_k} \sin(0.5\pi\beta_k)\right]^2}{\left[\sum_{r=0}^{n} a_r\, \omega_n^{\alpha_r} \cos(0.5\pi\alpha_r)\right]^2 + \left[\sum_{r=0}^{n} a_r\, \omega_n^{\alpha_r} \sin(0.5\pi\alpha_r)\right]^2}\right]^{1/2}, \quad (\mathbf{4.32})$$

$$\gamma = \text{Arctan}\frac{\sum_{k=0}^{n} b_k\,\omega_n^{\beta_k}\sin(0.5\pi\beta_k)}{\sum_{k=0}^{n} b_k\omega_n^{\beta_k}\cos(0.5\pi\beta_k)} - \arctan\frac{\sum_{r=0}^{n} a_r\,\omega_n^{\alpha_r}\sin(0.5\pi\alpha_r)}{\sum_{r=0}^{n} a_r\,\omega_n^{\alpha_r}\cos(0.5\pi\alpha_r)} - \theta\omega_d, \quad (\mathbf{4.33})$$

$$P = K_p\omega_n^{\lambda},\ I = K_i,\ D = K_d\omega_n^{\lambda+\mu}. \quad \mathbf{(4.34)}$$

Note that the direction of the inequality sign in Eq. (4.30) should be reversed if $|C_n| < 1$; further, if the equality sign is taken instead of the inequality sign this equation defines a surface (constant noise rejection surface C_n at frequency ω_n). If $\omega \geq \omega_n$, Eq. (4.7) will be satisfied on the side of this surface which will be defined in Chapter5.

In Eqs. (4.30) and (4.31), P, I, D are used instead of K_p, K_{pi}, K_d for programming easiness, see Chapter 5. If K_p, K_i, K_d are used the following inequality results

$$K_p^2\omega_n^{2\lambda} + K_i^2 + K_d^2\omega_n^{2(\lambda+\mu)} + 2K_pK_i\omega_n^{\lambda}\cos(0.5\pi\lambda) + 2K_pK_d\omega_n^{2\lambda+\mu}\cos(0.5\pi\mu)$$
$$+2K_dK_i\omega_n^{\lambda+\mu}\cos[0.5\pi(\lambda+\mu)] + \frac{2\omega_n^{\lambda}C_n^2}{N(C_n^2-1)}\Big[K_p\omega_n^{\lambda}\cos(\gamma) + K_i\cos(0.5\pi\lambda-\gamma) +$$
$$K_d\omega_n^{\lambda+\mu}\cos(0.5\pi\mu-\gamma)\Big] + \frac{\omega^{2\lambda}C_n^2}{N^2(C_n^2-1)} \geq 0. \quad \mathbf{(4.35)}$$

5. 3D PROGRAMMING IMPLEMENTATIONS

In this section, Programming details for the 3-D plots of the stability, flatness, disturbance and noise surfaces as well as the flatness curve are illustrated. The basic ideas for the preparation of the related function and their use are illustrated. The programs are prepared by using Matlab language.

5.1. Stability Surfaces

Consider Eq. (4.16) for CRB. For a mesh-grid structure for the variables K_p, K_i. The third line in Eq. (4.16) that is

$$\mathrm{f}\left[\left(\mathrm{K_p}, \mathrm{K_i}\right), \omega\right] = \mathrm{K_p}\omega^{\lambda}\sin(0.5\pi\mu) + \mathrm{K_i}\sin[0.5\pi(\lambda+\mu)] \pm \frac{\omega^{\lambda}}{\mathrm{N}}\sin(0.5\pi\lambda+\gamma) = 0 \quad \textbf{(5.1)}$$

should be satisfied for each grid point (K_p, K_i). When the frequency ω $f\left[\left(\mathrm{K_p}, \mathrm{K_i}\right), \omega\right]$ is scanned with convenient steps $\Delta\omega$ over a reasonable range, the frequencies satisfying Eq. (5.1) can be found by checking

$$\mathrm{f}\left[\left(\mathrm{K_p}, \mathrm{K_i}\right), \omega_{\mathrm{n-1}}\right] \cdot \mathrm{f}\left[\left(\mathrm{K_p}, \mathrm{K_i}\right), \omega_{\mathrm{n}}\right] \leq 0. \quad \textbf{(5.2)}$$

Whenever this equation is satisfied the solution of Eq. (5.1) for ω is thus found for the grid point (K_p, K_i) within an error $\pm\Delta\omega$. Then the second line of Eq. (4.16) can be used to find K_d as

$$K_d = \frac{\omega^{-\lambda}\mathrm{K_i}\sin(0.5\pi\lambda) \pm \frac{\sin(\gamma)}{\mathrm{N}}}{\omega^{\mu}\sin(0.5\pi\mu)} \quad (\mathbf{5.3})$$

which is the point on the stability surface corresponding to (K_p, K_i). 3-D Surface plot is obtained by the Matlab function "mesh".

RRB $K_i = 0$ is easy to plot since it is so simple.

We note that due to the transcendental nature of the function $f\left[\left(K_p, K_i\right), \omega\right]$and $\pm$ sign in it, Eq. (5.1) may have more than one solution. Each solution is considered as a separate stability surface and considered in the programming separately.

5.2. Flatness Surfaces

Consider Eqs. (4.17) and (4.18). For a mesh-grid structure for the variables $\mathrm{K_p}, \mathrm{K_i}$, Eq. (4.18) is solved for $\mathrm{K_d}$:

$$\mathrm{K_d}\left(\mathrm{K_p}, \mathrm{K_i}, \omega\right) = \frac{\frac{\omega^{\lambda+\mu}}{\mathrm{N}^2}\left(\theta - \psi_{\mathrm{spec}} - \frac{\mathrm{d}\beta}{\mathrm{d}\omega}\right) - \mathrm{K_p K_i}\lambda \sin(0.5\pi\lambda)}{\mathrm{K_p}\omega^{\lambda+\mu}\mu\sin(0.5\pi\mu) + \mathrm{K_i}(\lambda+\mu)\omega^{\mu}\sin[0.5\pi(\lambda+\mu)]}. \quad (\mathbf{5.4})$$

Substitute this K_d in Eq. (4.17) to obtain

$$\mathrm{f_f}\left[\left(\mathrm{K_p}, \mathrm{K_i}\right), \omega\right] = \mathrm{K_d^2}\left(\mathrm{K_p}, \mathrm{K_i}, \omega\right)\omega^{2(\lambda+\mu)} + \mathrm{K_d}\left(\mathrm{K_p}, \mathrm{K_i}, \omega\right)\left[2\mathrm{K_p}\omega^{2\lambda+\mu}\cos(0.5\pi\mu) + 2\mathrm{K_i}\omega^{\lambda+\mu}\cos\left(0.5\pi(\lambda+\mu)\right)\right] + \mathrm{K_p^2}\omega^{2\lambda} + \mathrm{K_i^2} + 2\mathrm{K_p K_i}\omega^{\lambda}\cos(0.5\pi\lambda) - \frac{\omega^{2\lambda}}{\mathrm{N}^2} = 0. \quad \mathbf{(5.5)}$$

This equation should be satisfied for each grid point (K_p, K_i). When the frequency ω is scanned with convenient steps $\Delta\omega$ over a reasonable range, the frequencies satisfying Eq. (5.5) can be found by checking

$$\mathrm{f_f}\left[\left(\mathrm{K_p}, \mathrm{K_i}\right), \omega_{\mathrm{n}-1}\right] \cdot \mathrm{f_f}\left[\left(\mathrm{K_p}, \mathrm{K_i}\right), \omega_{\mathrm{n}}\right] \leq 0. \quad (\mathbf{5.6})$$

Whenever this equation is satisfied the solution of Eq. (5.5) for ω is thus found for the grid point (K_p, K_i) within an error $\pm\Delta\omega$. Then Eq. (5.4) can be used to find $\mathrm{K_d}$ which is the point on the flatness surface corresponding to (K_p, K_i). 3-D Surface plot is obtained by the Matlab function "mesh".

We note that due to the transcendental nature of the function $f_f\{(K_p, K_i), \omega\}$ in Eq. (5.5) may have more than one solution. Each solution is considered as a separate flatness surface and at most four flatness surfaces are considered in the programming.

5.3. Flatness Curve

When the gain GCOF ω_{gc} (cross over frequency) is given and the flatness is specified at this frequency as in Eq. (4.23) (with an equality sign) then Eqs. (4.17) and (4.18) define

the flatness curve in the space (K_p, K_i, K_i) as already indicated in Section 4.2.2. To find the flatness curve we draw K_i from Eq. (4.18) to obtain

$$\mathrm{K_i} = \frac{\frac{\omega^{\lambda+\mu}}{\mathrm{N}^2}\left(\theta - \psi_{\mathrm{spec}} - \frac{\mathrm{d}\beta}{\mathrm{d}\omega}\right) - \mathrm{K_d K_p}\omega^{\lambda+\mu}\mu\sin(0.5\pi\mu)}{\mathrm{K_p}\lambda\sin(0.5\pi\lambda) + \mathrm{K_d}(\lambda+\mu)\omega^{\mu}\sin[0.5\pi(\lambda+\mu)]}. \qquad (\mathbf{5.7})$$

Substituting this in Eq. (4.17) and rearranging we obtain the following forth order polynomial equation in K_d:

$$\mathrm{q_4 K_d^4 + q_3 K_d^3 + q_2 K_d^2 + q_1 K_d + q_0 = 0}, \quad \text{where,} \qquad \mathbf{(5.8)}$$

$$\mathrm{q_4 = ag^2}, \quad \mathrm{q_3 = g(2fa + hc + bg)}, \quad \mathrm{q_2 = af^2 + fhc + 2gfb + efg^2}$$

$$\mathrm{q_1 = 2hH + gdH + fcH + fdh + bf^2 + 2gef}, \quad \mathrm{q_0 = fH^2 + fdH + ef^2},$$

$$a = \omega^{2\lambda+2\mu},\ b = 2K_p\omega^{2\lambda+\mu}\cos(0.5\pi\lambda),\ c = 2\omega^{\lambda+\mu}\cos[0.5\pi(\lambda+\mu)],$$

$$d = 2K_p\omega^{\lambda}\cos(0.5\pi\lambda), \quad e = K_p^2\omega^{2\lambda} - \frac{\omega^{2\lambda}}{N^2}, f = K_p\lambda\sin(0.5\pi\lambda),$$

$$g = \omega^{\mu}(\lambda+\mu)\sin[0.5\pi(\lambda+\mu)],\ h = -K_p\omega^{\lambda+\mu}\mu.H = -\frac{\omega^{\lambda+1}}{N^2}(\theta - \psi_{spec} - \frac{d\beta}{d\omega}).$$

Choosing a set of successive values of K_p, for each value find the roots of Eq. (5.8) for each value of $\mathrm{K_p}$, and then the corresponding values of K_i by using Eq. (5.7). Then 3D plot of (K_p, K_i, K_d) by using Matlab function "plot3". The function subprogram prepared for computing flatness curve is given and the results are shown in chapter 6 examples. In general Eq. (5.8) have 4 roots and only real roots of it are considered. Hence there may be more than one flatness curves.

5.4. Disturbance Rejection Surface

Consider Eq. (4.24) or Eq. (4.25) to find the surface on which the disturbance specification is satisfied with an equality sign. Then the disturbance specification will be satisfied on and on one side of this surface as implied by Eq. (4.29). Equation (4.25) can be arranged as a quadratic equation in the parameter D as follows:

$$D^2 + 2D\left[P\cos(0.5\pi\mu) + I\cos\{0.5\pi(\lambda+\mu)\} + \frac{\omega_d^{\lambda}}{N}\cos(0.5\pi\mu+\gamma)\right]$$

$$+\frac{2\omega_d^{\lambda}}{N}\left[P\cos(\gamma) + I\cos(0.5\pi\mu-\gamma) + \frac{\omega_d^{2\lambda}}{N^2}(1-\frac{1}{B_d^2})\right] = 0, \qquad \mathbf{(5.9)}$$

where N, γ, P, I, D are as defined in Eqs. (4.26), (4.27) and (4.28). Equation (5.9) is solved for each grid point of K_p, K_i. Then Eq. (4.28) is used to find $K_d = D/\omega_d^{(\lambda+\mu)}$. If a real root exists, then there are 2 solutions for D and hence for K_d, and the permissible region to satisfy Eq. (4.29) is outside of these roots. This corresponds to the outside of the two disturbance surfaces in the 3-D implementation obtained by the Matlab "mesh" function. The evaluation of the disturbance surfaces are conducted and shown by the examples given in Chapter 6.

5.5. Noise Rejection Surface

Noise rejection surface is defined by Eqs. (4.30) or (4.31) with the equality sign. Its equation is rewritten below in quadratic form in the parameter D.

$$\mathrm{D}^2 + 2\mathrm{D}\left[\mathrm{P}\cos(0.5\pi\mu) + \mathrm{I}\cos\{0.5\pi(\lambda+\mu)\} + \frac{\omega_\mathrm{n}^\lambda \mathrm{C}_\mathrm{n}^2}{\mathrm{N}(\mathrm{C}_\mathrm{n}^2-1)}\cos(0.5\pi\mu+\gamma)\right] + \mathrm{P}^2 + \mathrm{I}^2$$
$$+2\mathrm{PI}\cos(0.5\pi\lambda) + \frac{\omega_\mathrm{n}^\lambda \mathrm{C}_\mathrm{n}^2}{\mathrm{N}(\mathrm{C}_\mathrm{n}^2-1)}\left[2\mathrm{P}\cos(\gamma) + 2\mathrm{I}\cos(0.5\pi\lambda-\gamma) + \frac{\omega_\mathrm{n}^\lambda}{\mathrm{N}}\right] = 0, \quad \textbf{(5.10)}$$

where N, γ, P, I, D are as defined in Eqs. (4.32), (4.33), (4.34). Equation (5.10) is solved for each grid point of K_p, K_i. Then Eq. (4.34) is used to find $K_d = D/\omega_n^{(\lambda+\mu)}$. If a real root exists, then there are 2 solutions for D and hence for K_d, and the permissible region to satisfy Eq. (4.32) is inside of these roots (the case $|C_n| \leq 1$, otherwise outside). This corresponds to the inside of the two noise surfaces in the 3-D implementation obtained by the Matlab "mesh" function. The evaluation of the noise surfaces are conducted by matlab programming and the results are demonstrated in the next chapter.

5.6. Performance Characteristics

For any example with the FOPID controller and a rational FO plant transfer function with time constant time delay some performance characteristics are calculated and/or are plotted to verify the design results. This is done by the prepared function subprogram "performance". The outputs of this program are: Noise rejection variation with ω, Disturbance rejection variation with ω, Phase flatness variation with ω, Nichols chart for open loop gain, Polar plot for open loop gain, Nyquist plot for open loop gain, Gain and

phase plots (Bode diagrams) for open loop gain, Controller transfer function G_c, Plant transfer function $\mathrm{G_p}$, Open loop transfer function $G_c G_p$, Gain margins GM, g_m (in dB, and normal), Phase margins PM, φ_m (in degrees and radians), Phase crossover frequency ω_{pc}, and finally Gain crossover frequency ω_{pc}.

6. EXAMPLES

Examples presented in this section generally are taken as benchmark problems chosen from the literature and each one exhibits the theory in Section 4.2 and the programming aspects in Sections 5.1-5.6.

6.1. Example 1

Consider the experimental platform controlling liquid level in Basic Process Ring 38-100 Feedback Unit treated in (Monje et al, 2008). The plant (liquid level system) is characterized by the transfer function

$$\mathrm{G_p(s)} = \frac{3.13}{433.33\mathrm{s} + 1}\mathrm{e}^{-50\mathrm{s}} \qquad (\mathbf{6.1})$$

where dc gain is 3.13, time constant is 433.33 s and time delay is 50 s.

With the design specifications GCOF $\omega_{gc} = 0.008\, rad/s$, $PM\ \varphi_m = 60^o$, robustness to variations in the gain of the plant must be fulfilled *($\psi_{spec} = 0\ s\ at\ \omega_{gc}$),* sensitivity function $\leq B_d = -20\ dB\ for\ \omega \leq \omega_d = 0.001\, rad/s$, noise rejection $\leq C_n = -20\ dB$ for $\omega \geq \omega_n = 10\, rad/s$. In (Monje et al, 2008), the function FIMCON in the optimization toolbox of MATLAB is used to find the FOPID controller transfer function

$$\mathrm{G_c} = 0.6152 + \frac{0.01}{\mathrm{s}^{0.8968}} + 4.3867\mathrm{s}^{0.4773}. \qquad (\mathbf{6.2})$$

6.1.1. Performance characteristics

The control system performance is analyzed by the subprogram "performance"; the elapsed and CPU times are recorded as $1.6571s$ and $1.7188\ s$, respectively. The realized performance characteristics are satisfying the specified ones as seen in Table 6.1. Especially the ones indicated by '$+$' sign in the comment column fulfils the given design specifications.

Table 6. 1. Performance characteristics of $PI^{\lambda}D^{\mu}$ controlled liquid level system

Characteristics	Specification (*Not specified)	Realized	Comments: (--: No comment) =: Exact value , +: Satisfied value
ω_{gc} (rad/s)	0.008	0.008	=
PM (degrees)	60	60.0808	=
φ_m (rad)	1.0472	1.0486	
ψ_{spec} (s)	0	-0.0124	+
B_d	0.1	0.0706	+
B_d (dB)	-20	-23.0178	
ω_d (rad/s)	0.001	0.001	=
C_n	0.1	0.0099	+
C_n (dB)	-20	-40.1217	
ω_n (rad/s)	10	10	=
ω_{pc} (rad/s)	*	0.0392	--
GM (dB)	*	11.7541	_
g_m		3.8699	
Overshoot (%)	*	14.3	(Found by Simulink)
Rise time (s)	*	50+138	(from 10 % - to 90 %)
Settling time (s)	*	50+587	(95-105 % of final value)
Elapsed time	*	1.6571 s	--
CPU time	*	1.7188 s	--

The performance characteristics are illustrated by the plots shown in Figs. 6.1-6.7.

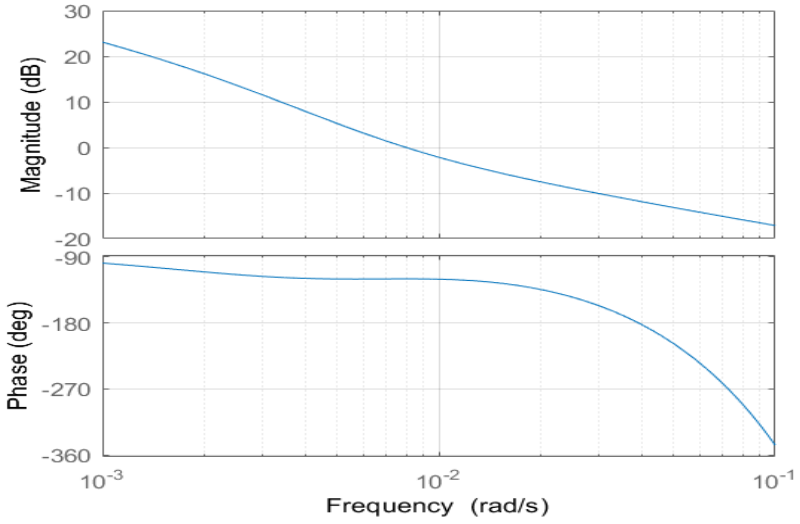

Figure 6. 1. Bode diagram of Example 6.1

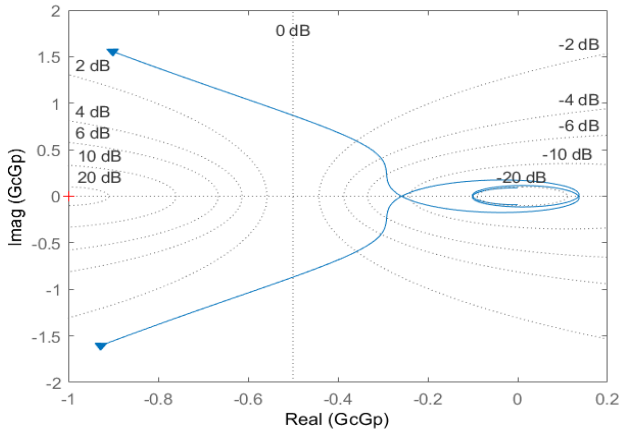

Figure 6. 2. Nyquist plot of Example 6.1

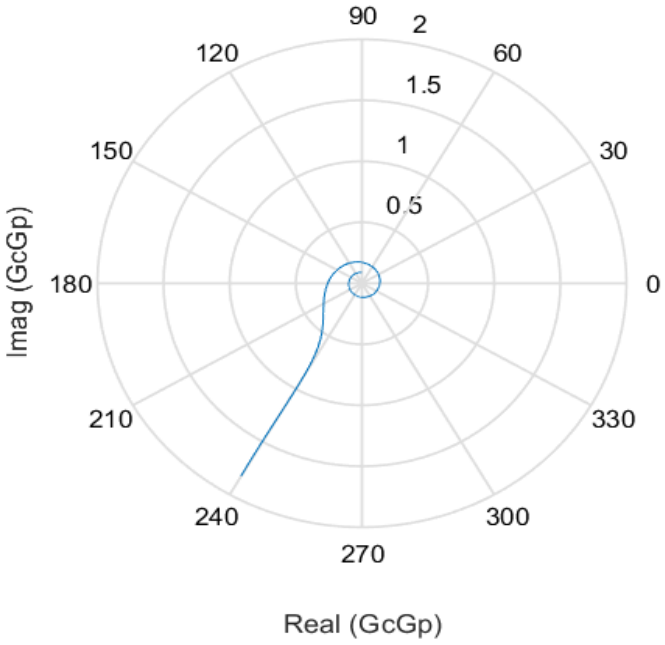

Figure 6. 3. Polar plot of Example 6.1

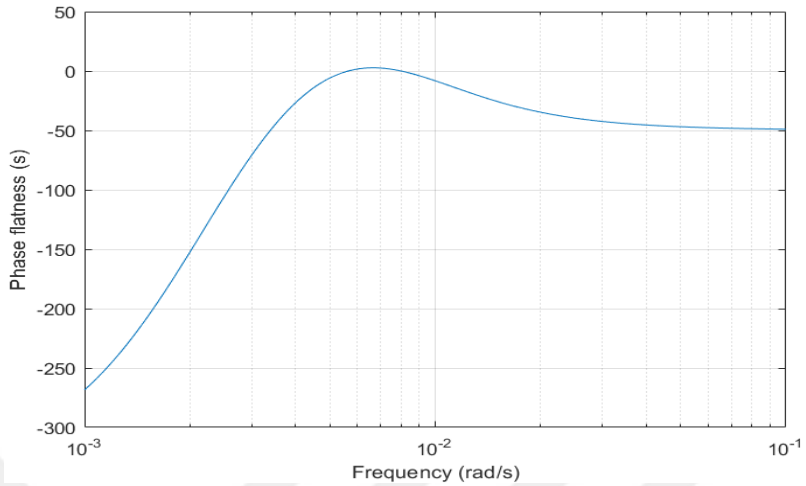

Figure 6. 4. Phase flatness curve of Example 6.1

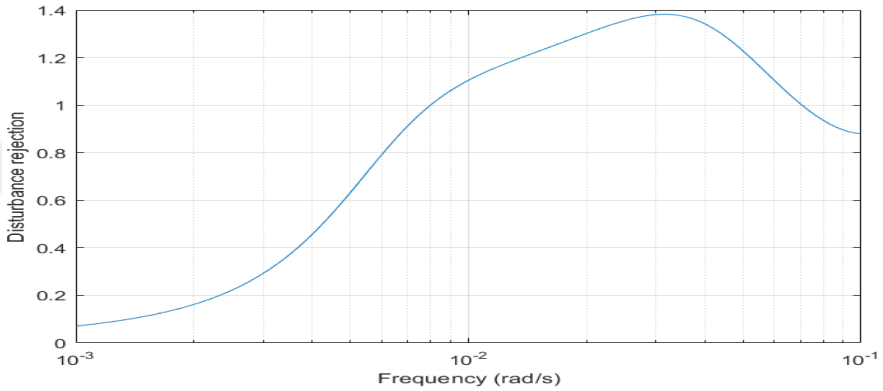

Figure 6. 5. Disturbance rejection curve of Example 6.1

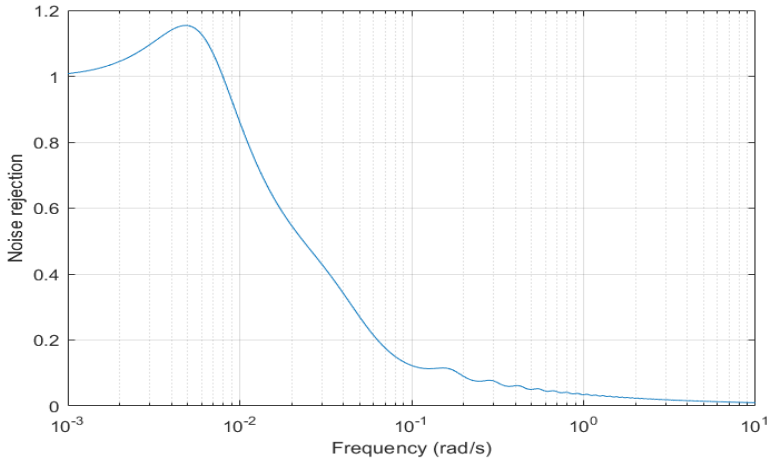

Figure 6. 6. Noise rejection curve of Example 6.1

Oustaloup continuous approximation (Oustaloup et al, 2000) is used with order $N = 5, \omega_b = 10^{-4}, \omega_h = 10^4\ rad/s$ for evaluation of step response by the FO Simulink blocks which appear in the FOTF Toolbox for FO system analyzer in Matlab (Xue, 2017). The function subprograms in this toolbox is also used for programming implementations presented in Chapter5. The resulting step response is shown in Fig. 6.7, and it has an overshoot of 14.3 %.

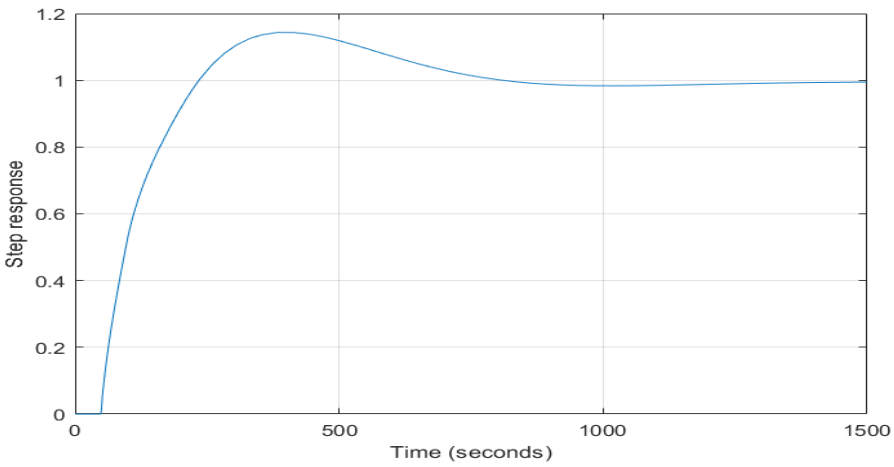

Figure 6. 7. Step response of closed loop system of Example 6.1

6.1.2. Disturbance and noise rejection boundaries

The disturbance rejection requirement is illustrated by the two boundary surfaces obtained by using matlab programing and the result of the 3D-plot is shown in Fig. 6.8. It is observed in this figure that the point $TP1 = (K_p, K_i, K_d)$ with the designed parameters of $PI^{\lambda}D^{\mu}$ controller is in the permissible region. Hence the disturbance rejection specification is satisfied. In fact in Table 6. 1, the transfer function $|T_D| = 0.0706$ which is less than the specified limit $B_d = 0.1\ at\ \omega_d = 0.001\ rad/s$, and $|T_D| \leq 0.1$ for all $\omega \leq \omega_d$. In Fig. 6.8, TP1 is the designed point. When the test point TP2 is taken between the boundary surfaces DBU and DBL as $TP2 = (K_p = 0.6, K_i = 0.002, K_d = 25)$, then the disturbance rejection specification will not be satisfied as expected; in fact, it is calculated that $|T_d| = 0.2464 \geq 0.1$ at $\omega_d = 0.001 rad/s$.

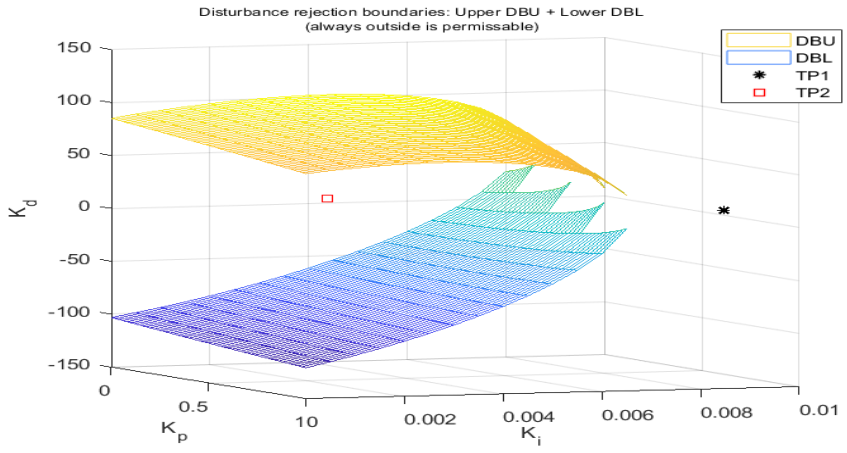

Figure 6. 8. Disturbance rejection boundaries and the test points of Example 6.1

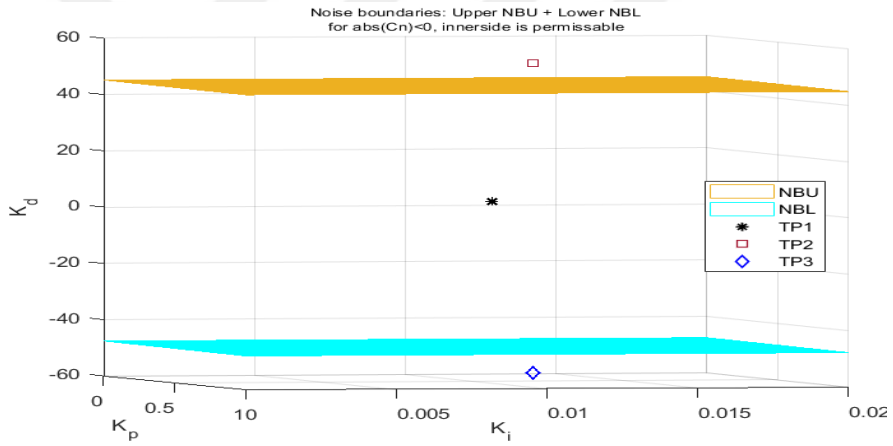

Figure 6. 9. Noise rejection boundaries and the test points of Example 6.1

When the noise specification is considered, Table 6.1 shows that noise rejection is well satisfied with the chosen controller parameters. In Fig. 6.9, noise rejection boundaries in 3-dimensional (K_p, K_i, K_d) space, which are obtained by using the matlab function and are shown with the test point TP1 of the designed controller. When the controller parameters are changed to $K_p = 0.9, K_i = 0.01, K_d = 55\ (-55)$, which correspond to the test point TP2 (TP3) shown in Fig. 6.9 (which is outside of the permissible region), then the noise transfer function takes the value $|T_N(j\omega_n)| = 0.1226\ (0.1144)$ which obviously, being greater than $C_n = 0.1$, violates the noise rejection specification.

6.1.3. Phase flatness curves and surfaces

Robustness to variations in the gain of the plant is satisfied by the phase flatness curve $\psi_f = 0\ at\ \omega_{gc}$. By choosing $\psi_{spec} = 0\ at\ \omega_{gc} = 0.008\ rad/s$ in Eq. (4.5), the flatness curve is obtained as shown in Fig. 6.10. Obviously the designed parameters fulfill this requirement (see the test point TP1). In fact $\psi_f = -0.0124 \cong 0$ at $\omega_{gc} = 0.008 rad/s$ and TP1 is almost on this curve. On the same figure, the phase flatness surface $\psi_f = 0$ without restricting the gain crossover frequency $\omega_{gc} = \omega_{gc}$ is also shown. It is naturally true that the phase flatness curve is on this surface as seen in the figure. Consider the two test points $TP2 = (K_p = 0.2, K_i = 0.018, K_d = 10)$ and $TP3 = (K_p = 0.5, K_i = 0.01, K_d = 18)$ which are inside and outside of the phase flatness boundaries. At TP3, it is found that $\psi_f = 41.9616\ s \gg 0\ at\ \omega_{gc} = 0.0093$ which is far away from $\psi_{spec} = 0$. At TP2, it is found that $\psi_f = -48.8777\ s \ll 0\ at\ \omega_{gc} = 0.0281$, which is far away from $\psi_{spec} = 0$ and being much negative, the relative stability is poor and the system may go to instability easily with uncertain plant parameters. So, the outer region of the phase flatness boundary is hardly desired design area. Note that the flatness curve data (FlatC1) is not in the visible range of the axis, and the phase flatness surfaces F3 and F4 do not exist for this example.

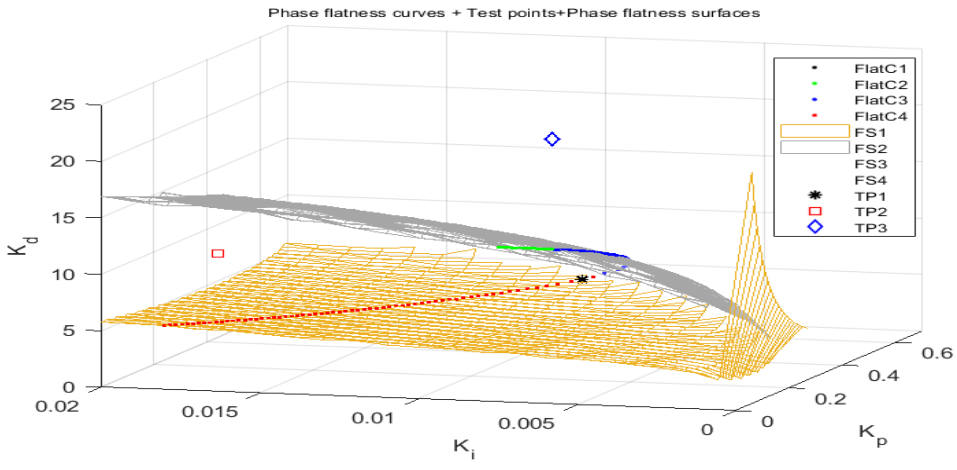

Figure 6. 10. Phase flatness curves and surfaces, and the test points

6.1.4. Complex root boundaries (CRB)

Complex root boundaries are plotted for a $GM = 11.7541\ dB (g_m = A = 3.8699)$ as realized by the design in (Monje et al, 2008) (see Table 1). As expected, due to the delay term of the plant transfer function and the transcendental behavior of the CRB equations treated in Section 5.1, there are multiple solutions for the boundary surface. Note that the designed system becomes unstable when the open loop gain is multiplied by the GM that is by $A = 3.8699$, which causes the Nyquist plot to pass from the critical point $(-1,0)$. Hence, the test point TP0 (*) should be on the CRB; this is in fact so as seen on the red surface CRBE2 in Fig. 6.11. In this figure, some other test points are indicated with blue squares (stable) and purple diamond (unstable) markers. The black hexagram $TP8 = (K_p = 0.6152, K_i = 0.01, K_d = 7.10)$ is a transition test point between stable and unstable cases (at TP8, $GM = -0.0026dB, PM = 0.0121\ rad/s$).

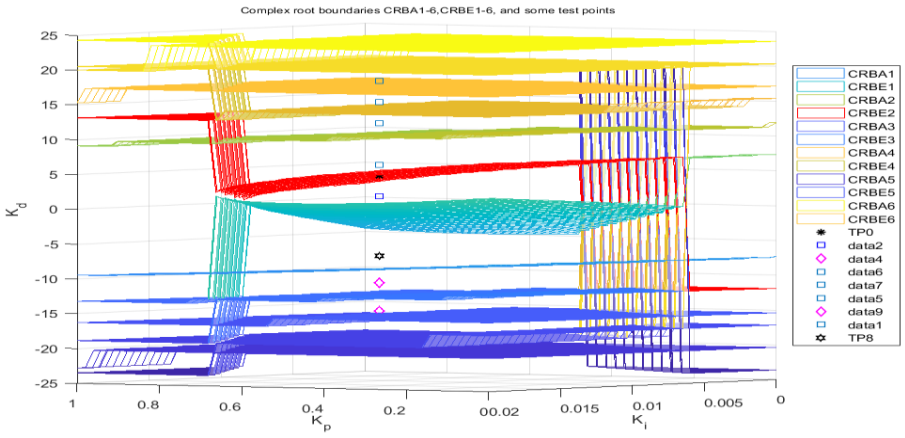

Figure 6. 11. Complex root boundaries and the test points of Example 6.1

The elapsed and CPU times are recorded as 17.0951 and 19.6719 s, respectively.

6.2. Example 2

Consider the benchmark problem treated as example 2 in (Zhao et al, 2005), fractional order plant model is given as (Podlubny, 1994):

$$G_p = \frac{1}{0.8s^{2.2} + 0.5s^{0.9} + 1}. \qquad (\mathbf{6.3})$$

According to the proposed method in (Zhao et al, 2005), it is selected that $\lambda = 0.1$ and $\mu = 1.15$ to achieve a $GM\ g_m = 1.3\ (2.2789\ dB)$ and $PM\ \varphi_m = 60^o$, then the controller parameters are determined as $K_p = 233.4234, K_i = 22.3972, K_d = 18.5274$. Thus, the controller transfer function is

$$G_c = 233.4234 + \frac{22.3972}{s^{0.1}} + 18.5274s^{1.15}$$
$$= \frac{18.5274s^{1.25} + 233.4234s^{0.1} + 22.3972}{s^{0.1}}. \qquad (\mathbf{6.4})$$

6.2.1. Performance characteristics

The performance characteristics of the designed control system is shown in Table 6.2. The elapsed and CPU times for running the subprogram "performance" are recorded as 3.1323 and 4.1719 s, respectively. The realized performance characteristics are satisfying the specified PM and GM as indicated by '+' in Table 6.2.

Table 6. 2. Performance characteristics of $PI^{\lambda}D^{\mu}$ controlled system of Example 6.2

Characteristics	Specification (*Not specified)	Realized	Comments: (--: No comment) =: Exact value , +: Satisfied value !: Can be improved
ω_{gc} (rad/s)	*	19.8601	--
PM (degrees)	60^o	60.9404	+
φ_m (rad)	1.0472	1.0636	!
ψ_f (s)	*	0.0244	!
B_d	*	0.3455	!
B_d (dB)		-9.2306	
ω_d (rad/s)	*	8	--
C_n	*	0.2657	!
C_n (dB)		-11.5114	
ω_n (rad/s)	*	70	--
ω_{pc} (rad/s)	*	Not defined	--
GM (dB)	2.2789	∞	+
g_m	1.3	∞	
Overshoot (%)	*	25.2	(Found by Simulink)
Rise time (s)	*	0.0707	(from 10 % - to 90 %)
Settling time (s)	*	0.4860	(95-105 % of final value)
Elapsed time (s)	*	3.1323	--
CPU time (s)	*	4.1719	--

Let us first check the realized parameters $\varphi_m, \psi_f, B_d, C_n, g_{,m}$ shown in Table 6.2 by verifying the 3-D plots. The stability boundaries, flatness curves and surfaces, disturbance and noise boundaries together with the test point $TP0 = (K_p = 233.4234, K_i = 22.3972, K_d = 18.5274)$ obtained with $g_m = 1, \varphi_m = 60^o, \omega_{gc} = 19.8601, \psi_{spec} = -0.0244\ s, B_d = 0.3455\ at\ \omega_d = 8, C_n = 0.2657 at\ \omega_n = 70$ are shown in Figs. 6.12, 6.14, 6.15, 6.16, respectively.

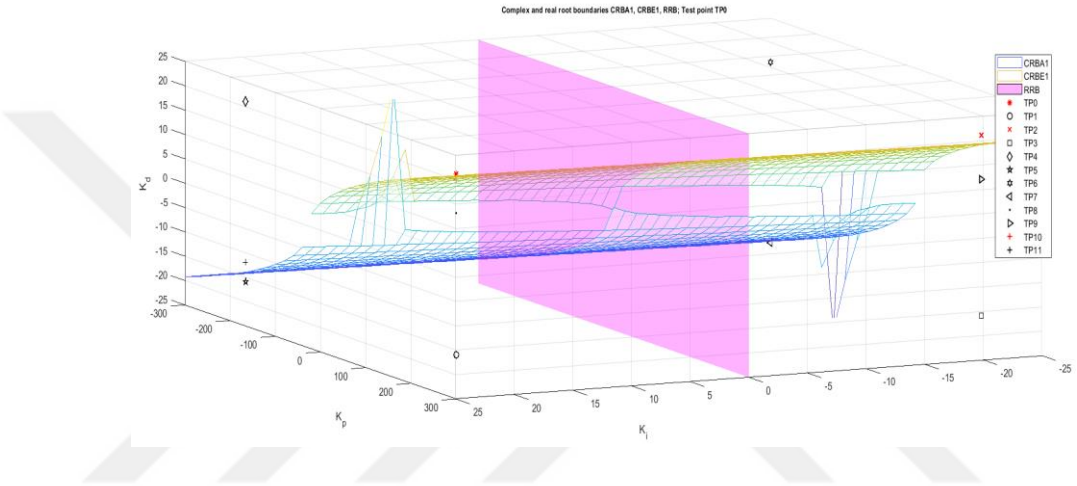

Figure 6. 12. Stability boundaries and the test points for Example 6.2

Table 6.3 shows the PMs and GMs calculated at some test points. It is seen that the test points TP5, TP7, TP11 are near the complex root boundary CRBA1. It worth's to remark first that CRBA1 is not the desired boundaries as mentioned at the end of Section 4.2.1; it is resulted due to the multivalued property of the solutions in Eqs. (4.15), (4.16), (5.1) and (5.3). In fact, at TP5, TP7, TP11, the PMs are computed as $-115.7367^o, -119.0596^o, -123.8282^o$, which are all near to -120^o; further, $tan(-120^o) = tan(60^o)$ and the inverse tangent function (which is used in Eq. (4.12) for example) can't differ at these arguments.

On the other hand, complex root boundary CRBE1, satisfies the property of PM crossing of 60^o; note that, in Table 6.3, the phases of TP0 and TP2 are above 60^o $(60.9404^o, 64.2633^o)$ whilst RP9 and TP10 result with PMs below 60^o $(31.6260^o, 58.2803^o)$.

Table 6. 3. Stability characteristics of test points for Example 6.2

Test Point	K_p	K_i	K_d	Marker	PM (degrees)	GM (dB)	Stability
TP0	$K_{p0} = 233.4234$	$K_{i0} = 22.3972$	$K_{d0} = 18.5274$	*	60.9404	∞	S
TP1	K_{p0}	K_{i0}	$-K_{d0}$	o	-75.8054	-50.3260	U
TP2	K_{p0}	$-K_{i0}$	K_{d0}	x	64.2633	∞	S
TP3	K_{p0}	$-K_{i0}$	$-K_{d0}$	⊓	-77.3033	-48.6125	U
TP4	$-K_{p0}$	K_{i0}	K_{d0}	Diamond	102.6967	-46.0955	U
TP5	$-K_{p0}$	K_{i0}	$-K_{d0}$	Pentagram	-115.7367	-46.1052	U
TP6	$-K_{p0}$	$-K_{i0}$	K_{d0}	Hexagram	104.1946	∞	U
TP7	$-K_{p0}$	$-K_{i0}$	$-K_{d0}$	<|	-119.0596	∞	U
TP8	K_{p0}	K_{i0}	10.5274	.	31.8576	-19.9537	U
TP9	K_{p0}	$-K_{i0}$	9.5274	>	31.6260	-23.1595	U
TP10	K_{p0}	K_{i0}	17.5274	+	58.2803	∞	S
TP11	$-K_{p0}$	K_{i0}	-15.5274	+	-123.8282	-46.1044	U

Having the positive GMs and PMs, test points TP0, TP2, TP10 correspond to a stable system, which is also verified by the obtaining the step responses shown in Fig. 6.13. All the other test points correspond to unstable systems. Since PM for $TP10 < 60^o$, the only test points among the shown in Table 6.3 remaining in the feasible stable region (stable region satisfying the given PM specification) are TP0 and TP2. The overshoots are measured as $26.9, 24.5$ % , and 28.5 % for TP0, TP2, TP10, respectively. This similarity between the overshoots are expected due to near PMs of values $60.9404^o, 64.2633^o, 58.2803^o$, respectively.

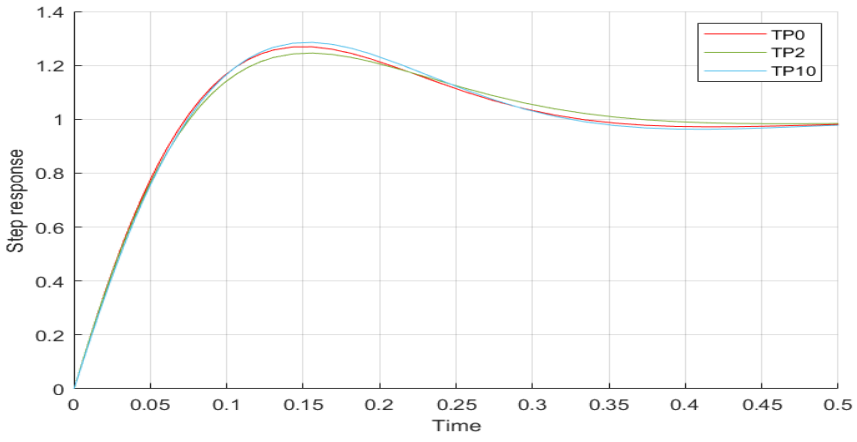

Figure 6. 13. Step responses for the test points TP0, TP2, TP10 of Example 6.2

6.2.2. Phase flatness curves and surfaces

Flatness curves and surfaces are shown in Figs. 6.14 and 6.15 which include some critical test points at which the relevant performance characteristics are shown in Table 6.4. The flatness curves and surfaces including the stability, disturbance and noise boundary plots are obtained and show on the Figs 6.14 and 6.15. Its time properties are elapsed time = $29.7287\ s$, CPU time = $48.6250\ s$.

The following observations are pointed out about the flatness plots:

i. On all the flatness curves FlatC1-FlatC4, $\psi_f = 0.0244$, which is the case it should be (see TP0-TP12).

ii. On all the flatness surfaces FS1-FS2, $\psi_f = 0.0244$ within 3 significant digits (see TP13, TP14). Since these points are not on the flatness curves $\omega_{gc} \neq 19.86$, it is $12.8061(24.2674)$ at TP13 (TP14).

iii. In particular, the test point TP0 lies on the flatness curve (FlatC2) and the flatness surface FS2; further the flatness curve FC2 is on the flatness surface FS2. Since the curves and surfaces are not drawn for the same range of the controller parameters, the complete coincidence cannot be observed on the figures.

iv. When the test point is out of the flatness curves and as a consequence of this on the flatness surfaces, the phase flatness deviates from $\psi_f = 0.0244$; for example, see the test points TP15, TP16, TP17, at which $\psi_f = -0.0198 < 0.0244, = 0.0461 > 0.0244$, $= -0.0198 < 0.0244$, respectively. That is face flatness requirement is satisfied between the face flatness surfaces FS1 and FS2, and it is not satisfied outside.

Table 6. 4. Phase flatness characteristics of some test points of Example 6.2

Test Point	K_p	K_i	K_d	ω_{gc}	ψ_f	GM (dB)	PM (degrees)	Stability
TP0	233.4234	22.3972	18.5274	19.8601	0.0244	∞	60.9404	S
TP1	265	-635.6	-21.21	19.8625	0.0244	-13.5713	-112.0665	U
TP2	135	-473.1	-20.53	19.8563	0.0244	-13.6652	-113.6843	U
TP3	-155	-117.1	-18.97	19.8600	0.0244	∞	-117.8024	U
TP4	-405	180.4	-17.51	19.8583	0.0244	-46.6953	-122.2076	U
TP5	160	603.3	7.42	19.8602	0.0244	1.1178	-1.6409	U
TP6	-100	972	7.262	19.8604	0.0244	4.1339	-6.5587	U
TP7	-80	943.8	7.269	19.8599	0.0244	3.9307	-6.2016	U
TP8	365	307.4	7.679	19.8607	0.0244	-2.0696	2.8195	S
TP9	-480	267.3	-17.04	19.8582	0.0244	-47.4766	-123.7497	U

Table 6.4. (Continue)

TP10	-135	-141.3	-19.08	19.8588	0.0244	∞	-117.4902	U
TP11	95	-423.5	-20.32	19.8565	0.0244	-151.3584	-114.2098	U
TP12	335	-723.7	-21.57	19.8647	0.0244	-109.6292	-111.2481	U
TP13	-240	26	-3.4	12.8061	0.0244	-46.1883	-179.2739	U
TP14	470	30	22.1	24.2674	0.0245	-27.8106	53.4259	S
TP15	233.4	22.4	30	20.1367	-0.0198	-49.7082	-69.5048	U
TP16	233.4	22.4	8	14.0624	0.0461	-14.0027	20.0876	S
TP17	233.4	22.4	-15	20.1367	-0.0198	-49.7082	-69.5048	U

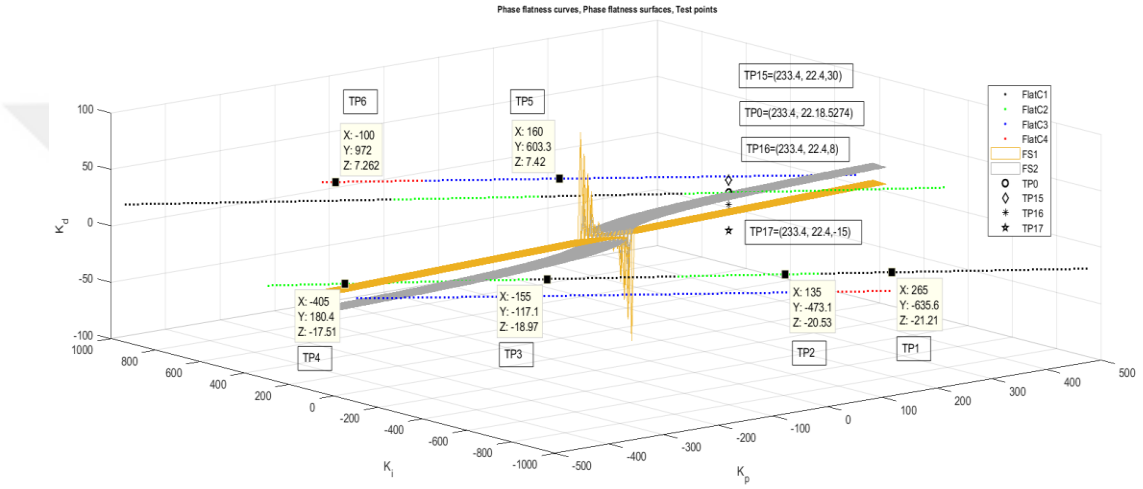

Figure 6. 14. Phase flatness curves and surfaces, and the test points TP0-TP6, TP15-TP17 of Example 6.2

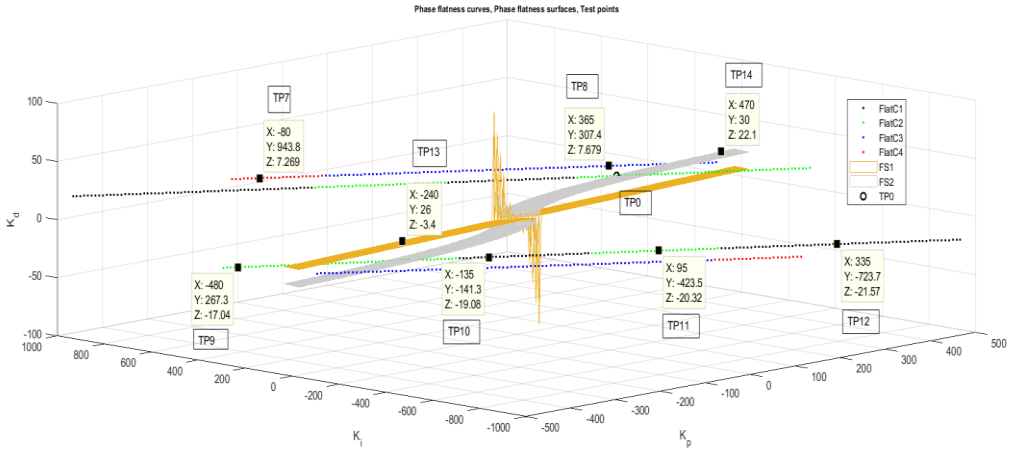

Figure 6. 15. Phase Flatness curves and surfaces, and the test points TP0-TP6 of Example 6.2

6.2.3. Disturbance rejection boundaries

Disturbance rejection boundaries including the test points tabulated in Table 6.5 are shown in Fig. 6.16. It is seen that the test point TP0 at which the disturbance is $B_d = 0.3455\ (-9.2306\ dB)\ at\ \omega_d = 8\ rad/s$ is on the disturbance boundary as expected. The disturbances at test points TP1, TP2, TP7 which are outside the boundary defined by the disturbance boundary surfaces DBU and DBL are computed as $-12.8050, -11.1968,$ and $-11.5875 dB$ which are all less than $-9.2306\ dB$, respectively. On the other hand, the disturbances at the test points TP3, TP4, TP5, TP6 which are all in the inner side of the disturbance boundary surfaces DBU and DBL are $-6.6959, 2.6749, 1.0445$ and $-7.3311\ dB$ which are greater than $-9.2306\ dB$, which means disturbance specification is not satisfied at these points. So, the theoretical results of Section 5.4 and the 3-D plot of disturbance rejection surfaces are well verified.

Table 6. 5. Disturbance characteristics of some test points for Example 6.2

Test Point	K_p	K_i	K_d	B_d (dB)a $\omega_d = 8$ r/s	C_n (dB)at $\omega_n = 70$r/s	ψ_f	PM (degrees)	GM (dB)	Stability
TP0	233.423	22.3972	18.5274	-9.2336	-11.5114	0.0244	60.3404	∞	S
TP1	320.1	34.88	26.24	-12.8050	-8.6298	0.0126	68.7722	∞	S
TP2	276.7	28.64	22.38	-11.1968	-9.9284	0.0173	65.4755	∞	S
TP3	190.1	16.16	14.68	-6.6559	-13.5019	0.0353	54.5864	∞	S
TP4	103.4	3.68	6.971	2.6749	-19.9733	0.0693	32.7970	∞	S
TP5	16.7	-8.8	-0.735	1.0445	-39.2671	-0.1353	-21.7298	−16.4517	S
TP6	-69.98	-21.28	-8.441	-7.3311	-18.6297	0.0664	-133.1718	∞	U
TP7	-156.7	-33.76	-16.15	-11.5875	-13.3019	0.0276	-118.3933	∞	U

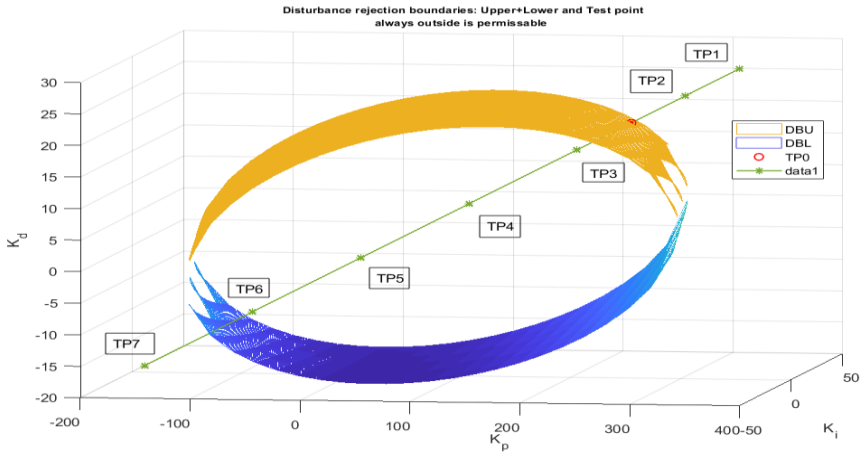

Figure 6. 16. Disturbance rejection surface and test points of Example 6.2

6.2.4. Noise rejection boundaries

Noise rejection boundaries including the test points tabulated in Table 6.6 are shown in Fig. 6.17. It is seen that the test point TP0 at which the noise gain is $C_n = 0.2657(-11.5114\ dB)\ at\ \omega = 70\ rad/s$ is on the noise boundary (NBU) as expected. The same property is valid for the test point TP7 which is on the lower boundary NBL. Being between the noise boundaries surfaces NBU and NBL, the test points TP2, TP3, TP4, and TP5 satisfy the noise rejection requirement since, the noise gains at these points are all smaller than the specified value at $-11.5114\ dB\ at\ \omega_n = 70\ rad/s$. The test point TP1which is above the noise boundary NBU does not satisfy the noise rejection requirement since, it yields a noise gain $-8.5031\ dB$ which is greater than the specified value $-11.5114\ dB$. Similarly, the test point TP6 which is below the noise boundary NBL does not satisfy the noise rejection requirement since, it yields a noise gain $-9.8731\ dB$ which is greater than the specified value $-11.5114\ dB$. As a result, the points remaining between the noise boundary surfaces NBU and NBL are the feasible points from the noise rejection point of views; and the points outside of these boundaries are not permissible.

So, the theoretical results of Section 5.5 and for 3-D plot of noise rejection surfaces are well verified.

Table 6. 6. Noise characteristics of some test points for Example 6.2

Test Point	K_p	K_i	K_d	B_d (dB)at $\omega_d = 8\ r/s$	C_n (dB)at $\omega_n = 70r/s$	ψ_f	PM (degrees)	GM (dB)	Stability
TP0	233.423	22.397	18.527	-9.2336	-11.5114	0.0244	60.3404	∞	S
TP1	230.1	31.88	26.84	-11.5581	-8.5031	0.0086	73.9958	∞	S
TP2	236.7	12.92	10.22	-7.1768	-16.6134	0.0486	31.0285	−19.9884	S
TP3	240	3.44	1.918	-6.8526	-29.2536	0.0120	−8.1255	11.1198	U
TP4	243.4	-6.04	-6.388	-8.6061	-19.7476	-0.0287	-44.1608	−46.8469	U
TP5	246.7	-15.52	-14.69	-10.9464	-13.2978	-0.0205	-69.3573	−48.4513	U
TP6	250	-25	-23	-13.0966	-9.8731	-0.0089	-81.8201	−49.7436	U
TP7	120	-4	-19.01	-10.1111	-11.5104	-0.0089	-84.4180	−46.3027	U

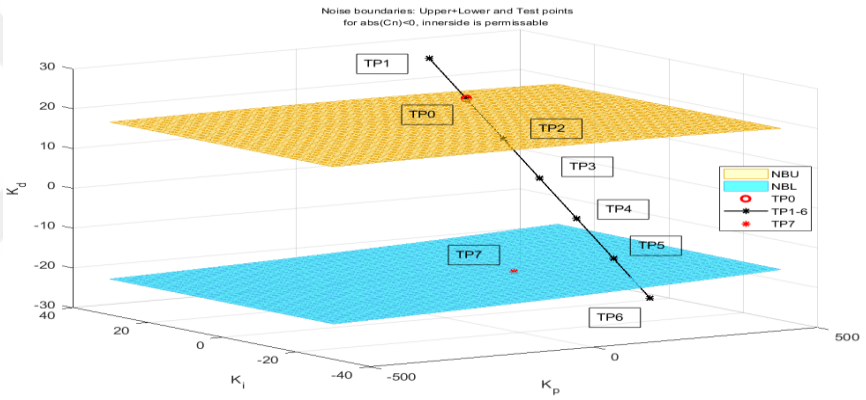

Figure 6. 17. Noise rejection boundaries, and the test points for Example 6.2

6.2.5. Composite 3D plottings

When the controller parameters are to be changed to obtain better performances than the specified ones, the new set of parameters should be chosen in the permissible regions defined by the individual plots. Therefore, a collection of the related boundaries is preferred on the same 3-D coordinate axis. For example, flatness, disturbance and noise are of concern, then the related boundaries are redrawn altogether as in Fig. 6.18 (flatness curves FC1, FC3, FC4 cannot be observed since they are out of the used scale) for the given example. Hence, a better design point (K_p, K_i, K_d) can be chosen by the use of Matlab 3D plotting facilities together with the subprogram "performance" to test the results. For example, the test point TP+ shown in this figure has design parameters $K_p = 310, K_i = 20, K_d = 15$ and it is in the permissible regions defined by the flatness,

disturbance and noise boundaries. Therefore, it is expected to give performance results better than the test point TP0; in fact flatness, disturbance rejection and noise rejection values of TP+ are $0.0382\ s, 10.5988\ dB, 13.2581\ dB$ which are all greater than those $0.0244\ s, 9.2336\ dB, 11.5114\ dB$ of TP0.

The composition is not restricted to the flatness, disturbance and noise plots only. Other 3D plots (stability boundaries, specified phase and gain margin boundaries) can also be combined among themselves or together with the above plots in a similar manner.

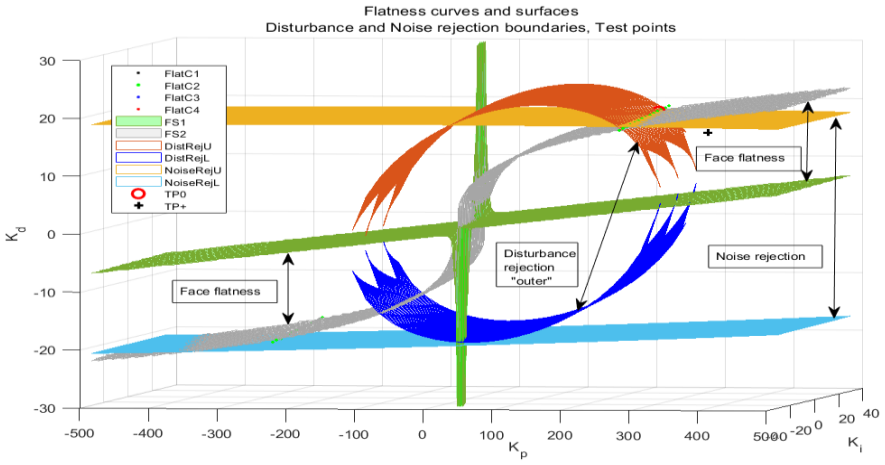

Figure 6. 18. Flatness, disturbance and noise boundaries on a single 3D plot of Example 6.2

6.3. Example 3

This example is taken from (Bhase and Patre, 2014), which presents a FOPI controller design for stabilizing the power control of a pressurized heavy water reactor. The reactor model is given by the transfer function

$$G_p(s) = \frac{1522.8947}{s^{2.0971} + 8.1944s^{1.0036} + 7.7684} e^{-2.0043\times10^{-12}s}. \qquad (6.5)$$

Design specifications are $PM\ \varphi_m = 90^o, GCOF\ w_{gc} = 0.3\ rad/s$ at which a flat phase satisfying $\psi_f = 0s$ is required. For this non-integer order plus time delay (NOPTD) plant, (Bhase and Patre, 2014) has obtained the following FOPI controller,

$$G_c(s) = 0.0016323 + \frac{0.001506}{s^{1.004}}. \qquad (6.6)$$

They claimed that their controller design approach provides better robust performance than other methods (Lee and Na, 2006; Das and Gupta, 2011).

The purpose of this example is to show how a PID controller design better than (Bhase and Patre, 2014) can be achieved by using 3-D methods presented in this thesis.

6.3.1. Performance characteristics

The performance characteristics of the control system designed by (Bhase and Patre, 2014) is shown in Table 6.7. The elapsed and CPU times for running the subprogram "performance" are recorded as $9.4474s$ and $7.2355s$, respectively. The realized performance characteristics are satisfying the specified PM as indicated by '+' in Table 6.7; so it is better the phase flatness ($0.0022 > 0$). The performance table is shown in the table below.

Table 6. 7. Performance characteristics of PI^{λ} controlled system of Example 6.3

Characteristics	Specification (*Not specified)	Realized	Comments: (--: No comment) =: Almost exact, +: Satisfied !: Can be improved
ω_{gc} (rad/s)	0.3	0.3003	=
PM (degrees)	90	90.0006	=
φ_m (rad)		1.5708	
ψ_f (s)	0	0.0022	+
B_d	*	0.1651	!
B_d (dB)		-15.6433	
ω_d (rad/s)	*	0.05	--
C_n	*	0.1159	!
C_n (dB)		-18.7212	
ω_n (rad/s)	*	3	--
ω_{pc} (rad/)	*	32.999	--
GM (dB)	*	55.6438	!
g_m		605.6060	
Overshoot (%)	*	0 %	(Found by Simulink)
Rise time (s)	*	7.2355	(from 10 % - to 90 %)
Settling time (s)	*	10.1088	(95-105 % of final value)
Elapsed time (s)	*	9.4474	--
CPU time (s)	*	9.2656	--

6.3.2. Complex root boundaries

For the modification of the designed PI^{λ} controller to obtain a proper PID controller, consider $PI^{\lambda=1.004}\,D^{\mu=1}$ first. The CRBs are drawn first. With $\lambda = 1.00$ and keeping $K_p = 0.0016323, K_i = 0.001506$ different K_d values tabulated in Table 6.8 are tested. Complex root boundaries and test points in the table are shown in Fig. 6.19.

Table 6. 8. Test points and the associated performance characteristics of Example 6.3

Test Point	K_d	C_n	B_d	ψ_f (s)	PM ($.^o$)	GM (dB)	ω_{gc} (rad/s)	Stability
TP1	0.050	0.9077	0.1793	-0.0023	87.4079	∞	52.4630	S
TP2	0.0351	0.8734	0.1749	-0.0044	89.9963	∞	38.0901	S
TP3	0.02	0.7967	0.1705	-0.0129	96.5714	∞	22.8036	S
TP0	0	0.1159	0.1651	0.0022	90.0006	55.6438	0.3003	S
TP4	-0.0048	44.3871	0.1639	-0.8276	77.4509	0.1772	0.5168	S
TP5	-0.0049	109.1646	0.1639	-0.2993	0.2673	0.0041	3.0149	S, U
TP6	-0.0050	48.0528	0.1638	-0.2598	-7.9166	-0.1627	3.5207	U
TP7	-0.020	1.3362	0.1601	-0.0132	-83.0231	-11.9591	22.8096	U
TP8	-0.0356	1.1653	0.1563	-0.0044	-89.9897	-16.9233	38.5833	U
TP9	-0.06	1.0920	0.1508	-0.0016	-93.5597	-21.4333	61.8681	U

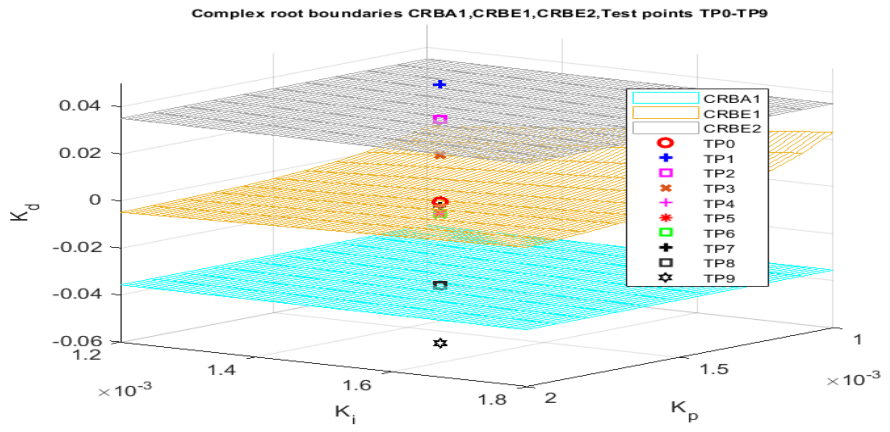

Figure 6. 19. Complex root boundaries and some test points of Example 6.3

The following observations are detected from the results of Fig. 6. 19 and Table 6.8.

i. Only 3 CRBs are observed in the 3D plots, CRBA1, CRBE1, and CRBE2. Since PM is measured as 90^o at TP2 and TP0 these are the actual feasible between which the

PM specification is satisfied. On the other hand, CRBA1 is not acceptable one since at TP8 (on CRBA1) the $PM \cong -90^o$ (not $+90^o$). As a result, the feasible region is bounded by the CRBE2 on the top, and by the CRBE1 at the bottom.

ii. The controlled system is unstable for $K_d < -0.0049$, hence the region below $K_d = -0.0049$ (so are the test points TP6-TP9) is out of interest. In facts these points yield both negative GM and PM.

iii. In the sense of phase flatness TP3 with $K_d = 0.02$ yields a better $PM(= 96^o > 90^o)$ then TP0 with $K_d = 0$, further, it yields a flatness over a larger range of frequencies around $\omega_{gc} = 22.8036\ \text{rad/s}$ (though the flatness is slightly less than that of TP0, it is still almost 0). Disturbance rejection properties are almost the same. Although TP0 has a higher noise suppression, this characteristic is as a design specification.

iv. Result: K_d should satisfy $0 \leq K_d \leq 0.0351$.

6.3.3. Phase flatness curves and surfaces

For discussing the phase flatness boundaries, the test points shown in Table 6.9 are considered. TP2 is on the flatness surface FS2 and TP0 is on the FS1 whilst TP3 is between these surfaces. See Fig. 6.20 where the flatness curves FC1 and FC2 do not exist for this example that is there are only 2 flatness curves. Hence, the phase requirement specification $\psi_f \geq 0.0022$ are satisfied for these test points. Note that the original design gives a phase flatness 0.0022, therefore the "0" phase flatness requirement is made more stringent by choosing 0.0022 instead of 0. TP1 and TP4 do not satisfy phase flatness requirement for having $\psi_f < 0.0022\ s$. Note that TP1 is above FS2 and TP4 is below FS1. Note also that TP0 is on the flatness curve (FlatC4) as well, which should be the case.

Result: K_d should satisfy $0 \leq K_d \leq 0.013$.

Table 6. 9. Test points for discussing the phase flatness boundaries and the associated performance characteristics of Example 6.3

Test Point	K_d	C_n	B_d	ψ_f (s)	PM ($.^o$)	GM (dB)	ω_{gc} (rad/s)	Stability
TP1*	0.02	0.7967	0.1705	-0.0129	96.5714	∞	22.8036	S
TP2	0.013	0.7175	0.1686	2.0175	95.8821	∞	0.2008	S
TP3	0.007	0.5759	0.1670	1.1140	94.1412	∞	0.2304	S
TP0	0	0.1159	0.1651	0.0022	90.0006	55.6438	0.3003	S
TP4	-0.010	1.9972	0.1626	-0.0509	-65.9491	-6.0306	11.6598	U

*Some of the data for TP1 is not reliable since there are 3 different ω_{gc}.

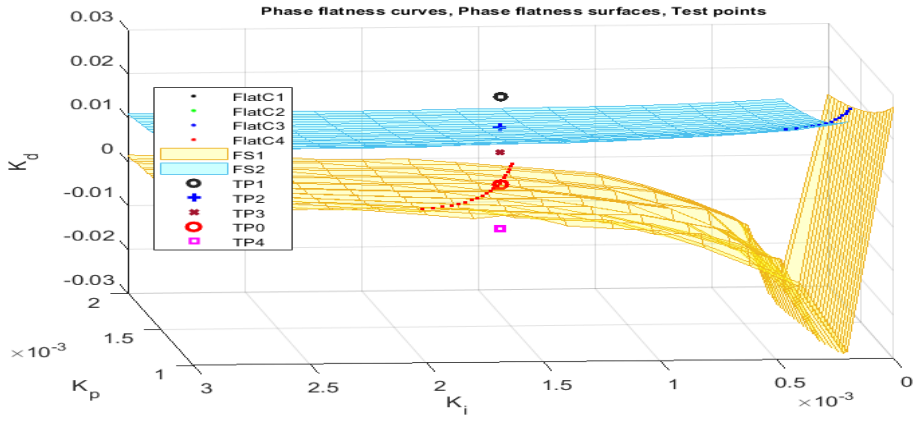

Figure 6. 20. Phase flatness curves and surfaces of Example 6.3

6.3.4. Noise boundaries

Noise boundaries are plotted in Fig. 6.21. The permissible region is between the boundary surfaces NBU and NBL. The designed system is at the test point TP0 which is on the surface NBL. The data for the test points on the figure are given in Table 6.10. It is observed that TP2, TP3 and TP0 satisfy the noise rejection requirement, and the test points TP1 and TP4 do not. The mentioned requirement is not a design specification, it is the limit by considering the determined by the PI^{λ} design by (Bhase and Patre 2014). Therefore the following result can be waived.

Result: K_d should satisfy $0 \leq K_d \leq 0.00045$.

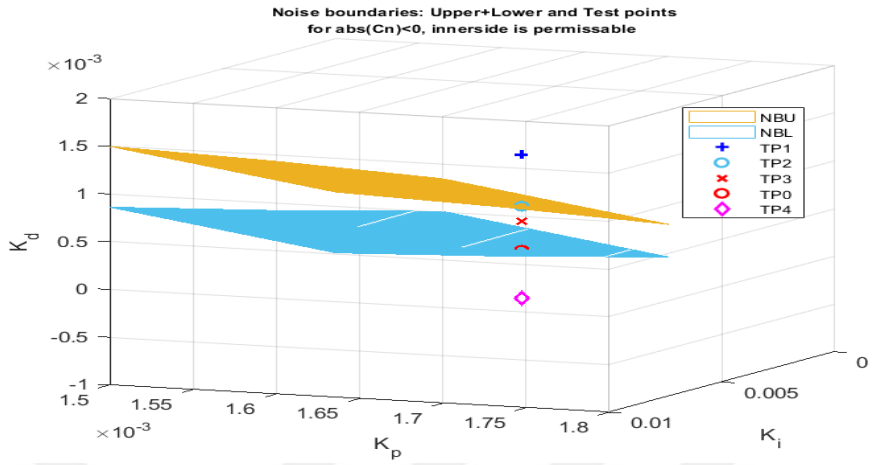

Figure 6. 21. Noise rejection boundary surfaces for Example 6.3

Table 6. 10. Test points for discussing the noise rejection boundaries and the associated performance characteristics for Example 6.3

Test Point	K_d	C_n	B_d	ψ_f (s)	PM ($.^o$)	GM (dB)	ω_{gc} (rad/s)	Stability
TP1	0.0010	0.1685	0.1654	0.1667	90.8924	∞	0.2852	S
TP2	0.00045	0.1144	0.1653	0.0765	90.4232	∞	0.2931	S
TP3	0.0003	0.1075	0.1652	0.0518	90.2866	∞	0.2954	S
TP0	0	0.1159	0.1651	0.0022	90.0006	55.6438	0.3003	S
TP4	-0.0005	0.1953	0.1650	-0.0810	89.4818	18.7161	0.3090	U

6.3.5. Disturbance boundaries

There is no disturbance specification given in the design problem. In fact, the disturbance rejection is hardly affected by the change of the parameter K_d. This is observed from the plots of the relevant boundaries which give a large region of permissible values for K_d. See also the results in Tables $6.4 - 6.6$ where B_d changes in the limits $\cong [0.16 - 0.18]$ only.

6.3.6. Step responses

The step responses of the original design with PI^{λ} controller and the suggested PID controller are shown in Fig. 6.22. The step response with a combination of PID and

PI Delay controller is also shown on the same figure. The critical time domain characteristics are indicated in Table 6.11.

It is observed that although the PID controller has better PM and GM values $(94.1412^o \; and \; \infty \; dB)$ than those $(90.0006^o \; and \; 55.6438 \; dB)$ of PI^{λ} controller (see Table 6.9), It has slightly higher rise time $T_r = 8.58 > 7.25$. Further, the phase flatness of PID controller is better than that of PI^{λ} controller, $\psi_f = 1.1140$ and 0.0022 s, respectively. There appear no overshoots in the step responses of both designs.

To reduce the rise and settling times a composite controller is suggested; the proposed controller is a PID in parallel with a PI controller which takes an action at $0.2 \; s \; (PI \; with \; 0.2 \; s \; Delay)$ as shown in Table 6.11. This composite controller has reduced the rise time and settling time to $0.27 \ll 7.25 \; s$ and $2.5 \ll 10 \; s$, respectively paying a tolerance of 1 % on the overshoot.

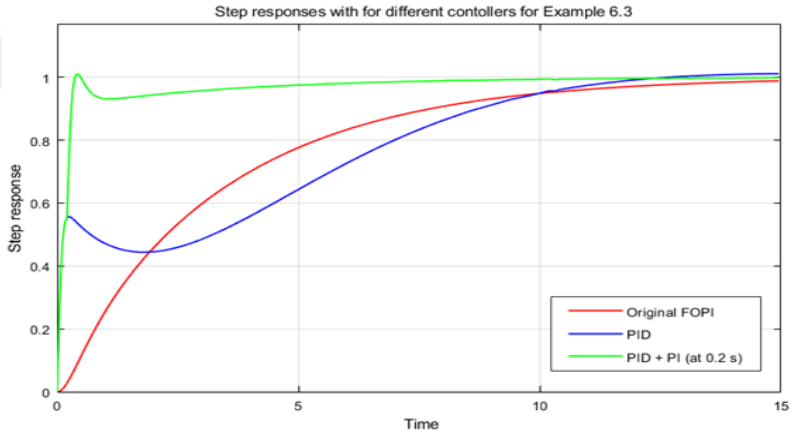

Figure 6. 22. Step responses of the system of Example 6.3 with different controllers

Table 6. 11. Time characteristics with the controllers $PI^{\lambda}, PID \; and \; PID + PI \; Delay$

Controller	K_p	K_i, λ	K_d, μ	T_r (s)	T_s (s)	Overshoot (%)
PI^{λ}	0.0016323	0.001506, 1.004	0, 0	7.25	10	0
PID	0.0016323	0.001506, 1	0.007, 1	8.58	10	0
(PID) + PI 0.2 s Delay	0.08	0.02, 1	0, 0	0.27	2.5	1

7. CONCLUSIONS

After a short introduction of the FOS, PID and FOPID controllers and giving the fundamental definitions and properties of fractional order calculus, important design methods of FOPID controllers are reviewed. And then the main topics of the thesis are considered in Chapters 4, 5, and 6. The frequency domain design specifications are given and frequency domain $PI^{\lambda}D^{\mu}$ control design formulas convenient for the 3D design method to realize these specifications are derived in Chapter 4. In particular, frequency domain characteristics such as stability boundaries to yield the required gain and phase margins, phase flatness surfaces and curves to achieve the required iso-damping property, boundary surfaces for low frequency disturbance rejection and high frequency noise rejection limits are considered. Chapter 5 illustrates how the derived formulas can be implemented for a computer programming yielding 3D plots usable in choosing design parameters.

The 3D plots and their use in designing ordinary PID or FOPID controllers have not been considered before in the literature on this extend. The method itself and different 3D plots are illustrated by examples in Chapter 6. The formulas derived in Chapter 4 and the 3D plots described in Chapter 5 are verified by these examples.

The presented method applies to control IO as well as FO plants with time delay by using $PI^{\lambda}D^{\mu}$ controllers, in particular by using any of $PI, PD, PI^{\lambda}, PD^{\mu}, PID$ controller.

FOTF toolbox (Xue, 2017) is used for preparing the subprograms to obtain the 3D plots of different surfaces and curves from the obtained formulas. The programs are written by using MATLAB notation. Oustaloup continuous approximation (Oustaloup et al, 2000) is used with order $N = 5, \omega_b = 10^{-4}, \omega_h = 10^4\ rad/s$ for evaluation of step response by the FO Simulink blocks which appear in the FOTF.

The main advantage of the presented 3D design method of $PI^{\lambda}D^{\mu}$ controllers is that one views in 3-D (K_p, K_i, K_d) space what ranges of the parameters can be used to achieve the required design specifications.

On behalf of its mentioned main advantage, there're are a few restrictions that can be listed as follows:

i. The method assumes the fractional orders λ and μ to be known. Never mind, these can be determined by other conventional design techniques reviewed and referred in the literature surveys of Section 1.3 and Chapter 3.

ii. Although the method is applicable for a large range of variety of plant transfer functions (FO or IO rational transfer functions with or without delay), it cannot be used for linear or nonlinear time varying plants, for stochastic plants and plants having hysteresis behavior.

iii. Since the formulas derived in this thesis are valid for any of $PI^{\lambda}D^{\mu}$ controllers and its abovementioned special forms, they cannot be used other controller designs such as $(PID)^{\lambda}$ (Lachhab et al, 2013), DOF FOPID (Vilanova and Visioli, 2018), TID (Tilt integral derivative, $P^{1/n}ID$) (Lurie, 1994), FO lead-lag (Tepljakov et al, 2018) controls.

There are a few points that should be cared on when using the presented 3D method of design of $PI^{\lambda}D^{\mu}$ controllers:

1. Due to the exponential (delay) term in the plant transfer function and due to the fractional orders in the transfer functions of the controller and/or plant as well as the multivalued solutions of some algebraic equations in the formulations, the boundaries computed for the stability, flatness, noise and disturbance rejections may be multiple. One has to decide which of them are true ones and which sides of these boundaries are permissible regions for the searched characteristics satisfying the given requirements. To decide this some test points should be tried by the program "performance" and the convenient regions should be chosen accordingly (Hamamci, 2008).

2. When the Nyquist plots of the open loop gain crosses negative real axis (multiple phase crossovers) and unity gain circle (multiple gain crossovers), improper GM and PM values may be resulted. This may occur when the plot travels in the right half plane due to the multiple values of inverse trigonometric functions (especially inverse tangent). One

should investigate the actual Bode plots given by “performance” instead of looking at the numerical results only; that is both the numerical results obtained by “performance” and the 3D plots used for different characteristics should be always judged.

Finally, similar derivations valid for the 3-D design of integer and/or fractional order controllers other than $PI^{\lambda}D^{\mu}$ controllers can be derived and there computer implementations can be programes as a future work.

8. REFERENCES

Ahmed, E., El-Sayed, A. M. A. and El-Saka, H. A. 2006. On some Routh–Hurwitz conditions for fractional order differential equations and their applications in Lorenz, Rössler, Chua and Chen systems. *Physics Letters A*, *358*: 1, 1-4..

Aldair, A. A. and Wang, W. J. 2010. Design of fractional order controller based on evolutionary algorithm for a full vehicle nonlinear active suspension systems. *International Journal of Control and Automation*, *3*: 4, 33-46..

Alfi, A. and Modares, H. 2011. System identification and control using adaptive particle swarm optimization. *Applied Mathematical Modelling*, *35*: 3, 1210-1221.

Ali, A. S., Radwan, A. G. and Soliman, A. M. 2013. Fractional order Butterworth filter: active and passive realizations. *IEEE journal on emerging and selected topics in circuits and systems*, *3*: 3, 346-354.

Åström, K. J. and Hägglund, T. 1995. *PID controllers: theory, design, and tuning* (Vol. 2). Research Triangle Park, NC: Instrument society of America.

Azar, A. T. and Serrano, F. E. 2018. Fractional order sliding mode PID controller/observer for continuous nonlinear switched systems with PSO parameter tuning. In *International Conference on Advanced Machine Learning Technologies and Applications* (pp. 13-22). Springer, Cham.

Bağış, A. and Senberber, H. 2016. Modeling of higher order systems using artificial bee colony algorithm. *An International Journal of Optimization and Control: Theories & Applications (IJOCTA)*, *6*: 2, 129-139.

Bhase, S. S, and Patre, B. M. 2014. Robust FOPI controller design for power control of PHWR under step-back condition. *Nuclear Engineering and Design*, *274*, 20-29.

Bingul, Z. 2004. A new PID tuning technique using differential evolution for unstable and integrating processes with time delay. In *International Conference on Neural Information Processing* (pp. 254-260). Springer, Berlin, Heidelberg.

Bingul, Z. and Karahan, O. 2012. Fractional PID controllers tuned by evolutionary algorithms for robot trajectory control. *Turkish Journal of Electrical Engineering and Computer Sciences*, 20: 1123-36.

Biswas, A., Das, S., Abraham, A. and Dasgupta, S. 2009. Design of fractional-order PIλDμ controllers with an improved differential evolution. *Engineering applications of artificial intelligence*, *22*: 2, 343-350.

Boudjehem, B. and Boudjehem, D. 2013. Fractional order controller design for desired response. *Proceedings of the Institution of Mechanical Engineers, Part I: Journal of Systems and Control Engineering*, *227*: 2, 243-251.

Cai, M., Pan, X. and Du, Y. 2009. New elite multi-parent crossover evolutionary optimization algorithm of parameters tuning of fractional-order PID controller and its application. In *2009 Fourth International Conference on Innovative Computing, Information and Control (ICICIC)* (pp. 64-67). IEEE.

Calderón, A. J., Vinagre, B. M. and Feliu, V. 2006. Fractional order control strategies for power electronic buck converters. *Signal Processing*, *86*: 10, 2803-2819.

Cao, J. Y. and Cao, B. G. 2006. Design of fractional order controllers based on particle swarm optimization. In *2006 1ST IEEE Conference on Industrial Electronics and Applications* (pp. 1-6). IEEE.

Cao, J. Y., Liang, J. and Cao, B. G. 2005. Optimization of fractional order PID controllers based on genetic algorithms. In *2005 international conference on machine learning and cybernetics* (Vol. 9, pp. 5686-5689). IEEE.

Caponetto, R. 2010. *Fractional order systems: modeling and control applications* (Vol. 72). World Scientific.

Chang, L. Y. and Chen, H. C. 2009. Tuning of fractional PID controllers using adaptive genetic algorithm for active magnetic bearing system. *WSEAS Trans. Syst*, *8*: 1, 158-167.

Charef, A., Sun, H. H., Tsao, Y. Y. and Onaral, B. 1992. Fractal system as represented by singularity function. *IEEE Transactions on automatic Control*, *37:* 9, 1465-1470.

Chen, Y., Hu, C. and Moore, K. L. 2003. Relay feedback tuning of robust PID controllers with iso-damping property. In *42nd IEEE International Conference on Decision and Control (IEEE Cat. No. 03CH37475)* (Vol. 3, pp. 2180-2185). IEEE.

Chopade, A. S., Khubalkar, S. W., Junghare, A. S., Aware, M. V. and Das, S. 2016. Design and implementation of digital fractional order PID controller using optimal pole-zero approximation method for magnetic levitation system. *IEEE/CAA journal of automatica sinica*, *5*: 5, 977-989.

Cokmez, E., Atiç, S., Peker, F. and Kaya, I. 2018. Fractional-order PI controller design for integrating processes based on gain and phase margin specifications. *IFAC-PapersOnLine*, *51*: 4, 751-756.

Dabiri, A., Moghaddam, B. P. and Machado, J. T. 2018. Optimal variable-order fractional PID controllers for dynamical systems. *Journal of Computational and Applied Mathematics*, *339*, 40-48.

Das, S., Das, S. and Gupta, A. 2011. Fractional Order Modeling of a PHWR Under Step-Back Condition and Control of Its Global Power With a Robust and Controller. *IEEE Transactions on Nuclear Science*, *58*:5, 2431-2441.

Das, S., Pan, I. and Das, S. 2013. Performance comparison of optimal fractional order hybrid fuzzy PID controllers for handling oscillatory fractional order processes with dead time. *ISA transactions*, *52:* 4, 550-566.

Das, S., Pan, I., Das, S. and Gupta, A. 2012. A novel fractional order fuzzy PID controller and its optimal time domain tuning based on integral performance indices. *Engineering Applications of Artificial Intelligence*, *25*: 2, 430-442.

Das, S., Saha, S., Das, S. and Gupta, A. 2011. On the selection of tuning methodology of FOPID controllers for the control of higher order processes. *ISA transactions*, *50*: 3, 376-388.

de Oliveira Valério, D. P. M. 2005. Fractional robust system control. *Universidade Técnica de Lisboa*.

Dimeas, I., Petras, I. and Psychalinos, C. 2017. New analog implementation technique for fractional-order controller: a DC motor control. *AEU-International Journal of Electronics and Communications*, *78*, 192-200.

El-Khazali, R. 2013. Fractional-order PIλDμ controller design. *Computers & Mathematics with Applications*, *66*: 5, 639-646.

El-Sayed, A. M. A., El-Mesiry, A. E. M. and El-Saka, H. A. A.. 2007. On the fractional-order logistic equation. *Applied Mathematics Letters*, *20*: 7, 817-823.

Fan, H., Sun, Y. and Zhang, X. 2007. Research on fractional order controller in servo press control system. In *2007 International Conference on Mechatronics and Automation* (pp. 2934-2938). IEEE.

Feliu-Batlle, V., Perez, R. R. and Rodriguez, L. S. 2007. Fractional robust control of main irrigation canals with variable dynamic parameters. *Control engineering practice*, *15*: 6, 673-686.

Ferreira, N. F. and Machado, J. T. 2003. Fractional-order hybrid control of robotic manipulators. In *Proc. 11th Int. Conf. Advanced Robotics, ICAR* (Vol. 1, pp. 393-398).

Franklin, G. F., Powell, J. D. and Workman, M. L. 1998. *Digital control of dynamic systems* (Vol. 3). Menlo Park, CA: Addison-wesley.

Freeborn, T. J., Maundy, B. and Elwakil, A. S. 2013. Cole impedance extractions from the step-response of a current excited fruit sample. *Computers and electronics in agriculture*, *98*, 100-108.

Ghasemi, S., Tabesh, A. and Askari-Marnani, J. 2014. Application of fractional calculus theory to robust controller design for wind turbine generators. *IEEE transactions on energy conversion*, *29*: 3, 780-787.

Hamamci, S. E. 2008. Stabilization using fractional-order PI and PID controllers. *Nonlinear Dynamics*, *51*: 1-2, 329-343.

Hamamci, S. E. 2007. An algorithm for stabilization of fractional-order time delay systems using fractional-order PID controllers. *IEEE Transactions on Automatic Control*, *52*:10, 1964-1969.

Hamamci, S. E. and Koksal, M. 2010. Calculation of all stabilizing fractional-order PD controllers for integrating time delay systems. *Computers & Mathematics with Applications*, *59*: 5, 1621-1629.

Hwang, C. and Cheng, Y. C. 2006. A numerical algorithm for stability testing of fractional delay systems. *Automatica*, *42*: 5, 825-831.

Jesus, I. S. and Machado, J. T. 2008. Fractional control of heat diffusion systems. *Nonlinear Dynamics*, *54*: 3, 263-282.

Kaczorek, T. 2008. Fractional positive continuous-time linear systems and their reachability. *International Journal of Applied Mathematics and Computer Science*, *18*: 2, 223-228.

Kadiyala, V. K., Jatoth, R. K. and Pothalaiah, S. 2009. Design and implementation of Fractional Order PID controller for aerofin control system. In *2009 World Congress on Nature & Biologically Inspired Computing (NaBIC)* (pp. 696-701). IEEE.

Kheirizad, I., Jalali, A. A. and Khandani, K. 2012. Stabilization of fractional-order unstable delay systems by fractional-order controllers. *Proceedings of the Institution of Mechanical Engineers, Part I: Journal of Systems and Control Engineering*, *226*: 9, 1166-1173.

Kheirizad, I., Khandani, K. and Jalali, A. A. 2013. Stabilisability analysis of high-order unstable processes by fractional-order controllers. *International Journal of Control*, *86*: 2, 244-252.

Lachhab, N., Svaricek, F., Wobbe, F. and Rabba, H. 2013. Fractional order PID controller (FOPID)-toolbox. In *2013 European control conference (ECC)* (pp. 3694-3699). IEEE.

Lee, C. H. and Chang, F. K. 2010. Fractional-order PID controller optimization via improved electromagnetism-like algorithm. *Expert Systems with Applications*, *37*: 12, 8871-8878.

Lee, Y. J. and Na, M. G. 2006. Robust controller design for the nuclear reactor power by extended frequency response method. *Nuclear Engineering and Technology*, *38*: 6, 551-560.

Li, H. and Chen, Y. 2008. A fractional order proportional and derivative (FOPD) controller tuning algorithm. In *2008 Chinese Control and Decision Conference* (pp. 4059-4063). IEEE.

Li, H., Luo, Y. and Chen, Y. 2009. A fractional order proportional and derivative (FOPD) motion controller: tuning rule and experiments. *IEEE Transactions on control systems technology*, *18:* 2, 516-520.

Li, Y., Ang, K. H. and Chong, G. C. 2006. PID control system analysis and design. *IEEE Control Systems Magazine*, *26*: 1, 32-41.

Luo, J., Nikolic, K., Evans, B. D., Dong, N., Sun, X., Andras, P. and Degenaar, P. 2016. Optogenetics in Silicon: A neural processor for predicting optically active neural networks. *IEEE transactions on biomedical circuits and systems*, *11*: 1, 15-27.

Luo, Y., Chen, Y. Q., Wang, C. Y. and Pi, Y. G. 2010. Tuning fractional order proportional integral controllers for fractional order systems. *Journal of Process Control*, *20*: 7, 823-831.

Lurie, B. J. 1994. Three-parameter tunable tilt-integral-derivative (TID) controller.

Ma, C. and Hori, Y. 2004. Fractional order control and its application of pi/sup/spl alpha//d controller for robust two-inertia speed control. In *The 4th International Power Electronics and Motion Control Conference, 2004. IPEMC 2004.* (Vol. 3, pp. 1477-1482). IEEE.

Maiti, D., Acharya, A., Chakraborty, M., Konar, A. and Janarthanan, R. 2008. Tuning PID and PI/λ D δ controllers using the integral time absolute error criterion. In *2008 4th International Conference on Information and Automation for Sustainability* (pp. 457-462). IEEE.

Maiti, D., Acharya, A., Chakraborty, M., Konar, A. and Janarthanan, R. 2008. Tuning PID and PI/λ D δ controllers using the integral time absolute error criterion. In *2008 4th International Conference on Information and Automation for Sustainability* (pp. 457-462). IEEE.

Maiti, D., Biswas, S. and Konar, A. 2008. Design of a fractional order PID controller using particle swarm optimization technique. *arXiv preprint arXiv:0810.3776*.

Manabe, S. 1960. The non-integer integral and its application to control systems. *Journal of Institute of Electrical Engineers of Japan*, *80*: 860, 589-597.

Mete, S., Ozer, S. and Zorlu, H. 2016. System identification using Hammerstein model optimized with differential evolution algorithm. *AEU-International Journal of Electronics and Communications*, *70*: 12, 1667-1675.

Monje, C. A., Vinagre, B. M., Feliu, V. and Chen, Y. 2008. Tuning and auto-tuning of fractional order controllers for industry applications. *Control engineering practice*, *16*: 7), 798-812.

Nakagawa, M. and Sorimachi, K. 1992. Basic characteristics of a fractance device. *IEICE Transactions on Fundamentals of Electronics, Communications and Computer Sciences*, *75*: 12, 1814-1819.

Oustaloup, A., Levron, F., Mathieu, B. and Nanot, F. M. 2000. Frequency-band complex noninteger differentiator: characterization and synthesis. *IEEE Transactions on Circuits and Systems I: Fundamental Theory and Applications*, *47*: 1, 25-39.

Oustaloup, A., Sabatier, J., Lanusse, P., Malti, R., Melchior, P., Moreau, X. and Moze, M. 2008. An overview of the CRONE approach in system analysis, modeling and identification, observation and control. *IFAC Proceedings Volumes*, *41*: 2, 14254-14265.

Özbay, H., Bonnet, C. and Fioravanti, A. R. 2012. PID controller design for fractional-order systems with time delays. *Systems & Control Letters*, *61*: 1, 18-23.

Padula, F. and Visioli, A. 2011. Tuning rules for optimal PID and fractional-order PID controllers. *Journal of process control*, *21*: 1, 69-81.

Pan, I. and Das, S. 2012. Chaotic multi-objective optimization based design of fractional order PIλDμ controller in AVR system. *International Journal of Electrical Power & Energy Systems*, *43*: 1, 393-407.

Pan, I. and Das, S. 2013. Enhancement of fuzzy PID controller with fractional calculus. In *Intelligent Fractional Order Systems and Control* (pp. 159-193). Springer, Berlin, Heidelberg.

Petras, I., Dorcak, L., O'Leary, P., Vinagre, B. M. and Podlubny, I. 2000. The modelling and analysis of fractional-order control systems in frequency domain. *arXiv preprint math/0008186*.

Podlubny, I. 1998. *Fractional differential equations: an introduction to fractional derivatives, fractional differential equations, to methods of their solution and some of their applications* (Vol. 198). Elsevier.

Podlubny, I. 1999. Fractional-order systems and PI/sup/spl lambda//D/sup/spl mu//-controllers. *IEEE Transactions on automatic control*, *44*: 1, 208-214.

Rajasekhar, A., Abraham, A. and Pant, M. 2014. A hybrid differential artificial bee colony algorithm based tuning of fractional order controller for permanent magnet synchronous motor drive. *International Journal of Machine Learning and Cybernetics*, *5*: 3, 327-337.

Rajasekhar, A., Das, S. and Suganthan, P. N. 2012. Design of fractional order controller for a servohydraulic positioning system with micro artificial bee colony algorithm. In *Congress on Evolutionary Computation* (pp. 1-8). IEEE.

Rajasekhar, A., Jatoth, R. K. and Abraham, A. 2014. Design of intelligent PID/PIλDμ speed controller for chopper fed DC motor drive using opposition based artificial bee colony algorithm. *Engineering Applications of Artificial Intelligence*, *29*, 13-32.

Ren, H. P., Fan, J. T. and Kaynak, O. 2018. Optimal design of a fractional order PID controller for a pneumatic position servo system. *IEEE Transactions on Industrial Electronics*.

Saha, D., Mondal, D. and Sen, S. 2013. Effect of initialization on a class of fractional order systems: experimental verification and dependence on nature of past history and system parameters. *Circuits, Systems, and Signal Processing*, *32:* 4, 1501-1522.

Salam, M. T., Velazquez, J. L. P. and Genov, R. 2015. Seizure suppression efficacy of closed-loop versus open-loop deep brain stimulation in a rodent model of epilepsy. *IEEE Transactions on Neural Systems and Rehabilitation Engineering*, *24*: 6, 710-719.

Sánchez, H. S., Padula, F., Visioli, A. and Vilanova, R. 2017. Tuning rules for robust FOPID controllers based on multi-objective optimization with FOPDT models. *ISA transactions*, *66*, 344-361.

Schlegel, M. and Čech, M. 2004. Fractal System Identification For Robust Control–The Moment Approach. *Department of Cybernetics, University of West Bohemia in Pilsen Univerzitn, Pilsen*.

Schultz, W. C. and Rideout, V. C. 1961. Control system performance measures: Past, present, and future. *IRE Transactions on Automatic Control* :1, 22-35.

Senberber, H. and Bagis, A. 2017. Fractional PID controller design for fractional order systems using ABC algorithm. In *2017 Electronics* (pp. 1-7). IEEE.

Senberber, H. and Bagis, A. 2018. ABC Algorithm Based System Modelling for Tuning the Fractional Order PID Controllers. *Elektronika ir Elektrotechnika*, *24*: 5, 3-9.

Shah, P. and Agashe, S. D. 2013. Design and optimization of fractional PID controller for higher order control system. In *International conference of IEEE ICART* (pp. 588-592).

Soltan, A., Xia, L., Jackson, A., Chester, G. and Degenaar, P. 2018. Fractional order PID system for suppressing epileptic activities. In *2018 IEEE International Conference on Applied System Invention (ICASI)* (pp. 338-341). IEEE.

Tan, N., Kaya, I., Yeroglu, C. and Atherton, D. P. 2006. Computation of stabilizing PI and PID controllers using the stability boundary locus. *Energy Conversion and Management*, *47*: 18-19, 3045-3058.

Tavazoei, M. S. 2010. Notes on integral performance indices in fractional-order control systems. *Journal of Process Control*, *20*: 3, 285-291.

Tepljakov, A., Alagoz, B. B., Yeroglu, C., Gonzalez, E., HosseinNia, S. H. and Petlenkov, E. 2018. FOPID controllers and their industrial applications: A survey of recent results. In *Proceedings of the 3rd IFAC Conference on Advances in Proportional-Integral-Derivative Control, Ghent, Belgium* (pp. 9-11).

Valerio, D. and Da Costa, J. S. 2004. Ninteger: a non-integer control toolbox for MatLab. *Proceedings of fractional differentiation and its applications, Bordeaux*.

Varol, H. A. and Bingul, Z. 2004. A new PID tuning technique using ant algorithm. In *Proceedings of the 2004 American control conference* (Vol. 3, pp. 2154-2159). IEEE.

Veronesi, M. and Visioli, A. 2010. Performance assessment and retuning of PID controllers for integral processes. *Journal of Process Control, 20*: 3, 261-269.

Meneses, H., Guevara, E., Arrieta, O., Padula, F., Vilanova, R. and Visioli, A. 2018. Improvement of the Control System Performance based on Fractional-Order PID Controllers and Models with Robustness Considerations. *IFAC-PapersOnLine*, *51*:4, 551-556.

Vinagre, B. M., Monje, C. A., Calderón, A. J. and Suárez, J. I. 2007. Fractional PID controllers for industry application. A brief introduction. *Journal of Vibration and Control*, *13*: 9-10, 1419-1429.

Wang, J., Niebur, E., Hu, J. and Li, X. 2016. Suppressing epileptic activity in a neural mass model using a closed-loop proportional-integral controller. *Scientific reports*, *6*, 27344.

Xue, D. 2017. *Fractional-order control systems: fundamentals and numerical implementations* Walter de Gruyter GmbH and Co KG (Vol. 1), Berlin

Xue, D., Zhao, C. and Chen, Y. 2006. Fractional order PID control of a DC-motor with elastic shaft: a case study. In *American control conference* (pp. 6-pp). IEEE.

Yüce, A., Tan, N. and Atherton, D. P. 2016. Fractional order pi controller design for time delay systems. *IFAC-PapersOnLine, 49*: 10, 94-99.

Zamani, M., Karimi-Ghartemani, M., Sadati, N. and Parniani, M. 2009. Design of a fractional order PID controller for an AVR using particle swarm optimization. *Control Engineering Practice, 17*: 12, 1380-1387.

Zhao, C., Xue, D. and Chen, Y. 2005. A fractional order PID tuning algorithm for a class of fractional order plants. In *IEEE International Conference Mechatronics and Automation* (Vol. 1, pp. 216-221). IEEE.

Zheng, W., Luo, Y., Wang, X., Pi, Y. and Chen, Y. 2017. Fractional order PIλDμ controller design for satisfying time and frequency domain specifications simultaneously. *ISA transactions, 68*, 212-222.

RESUME

Name and Surname:	Mohamed Hassan Nor
Birth place:	Mogadishu, Somalia
Date of Birth:	11/03/1991
Foreign Languages:	English, Turkish, Arabic
E-mail:	lagujaray@gmail.com

Education status

High school: Mogadishu Boarding Secondary School. Mogadishu, Somalia (2011).

Undergraduate: Mevlana University, Department of Electrical and Electronics Engineering (2016).